Research Square

Preprints are preliminary reports that have not undergone peer review.
They should not be considered conclusive, used to inform clinical practice,
or referenced by the media as validated information.

Photochemically synthesized silver nanoparticles form Banana flowers: Biological potential, phytochemical profiling and molecular docking insights

Humaira Rizwana
hrizwana@ksu.edu.sa
KING SAUD UNIVERSITY
Atiqa Riaz
KING SAUD UNIVERSITY
Rawan M. Alshalan
KING SAUD UNIVERSITY
Arwa Ahmad Alturki
KING SAUD UNIVERSITY
Horiah A. Aldehaish
KING SAUD UNIVERSITY
Ramesa Shafi Bhat
KING SAUD UNIVERSITY

Article

Keywords: Banana flowers, Saudi Arabia, postharvest fungi, AgNPs, sunlight, antifungal, cytotoxic, molecular docking

Posted Date: November 26th, 2026

DOI: https://doi.org/10.21203/rs.3.rs-11732226/v1

License: This work is licensed under a Creative Commons Attribution 4.0 International License.
Read Full License

Additional Declarations: No competing interests reported.

Photochemically synthesized silver nanoparticles form Banana flowers: Biological potential, phytochemical profiling and molecular docking insights.

Humaira Rizwana [1]*, Atiqa Riaz[1], Rawan M. Alshalan[1]; Arwa Ahmad Alturki[1], Horiah A. Aldehaish[1], Ramesa Shafi Bhat[2].
[1]Affiliation: Department of Botany and Microbiology, College of Science, King Saud University, Riyadh 11451, Saudi Arabia. hrizwana@ksu.edu.sa (H.R); 445206492@student.ksu.edu.sa (A.R); ralshalaan@ksu.edu.sa (R.M.S.); 439201288@student.ksu.edu.sa (A.A.T); haldehish@ksu.edu.sa (H.A.D).
[2]Affiliation: Biochemistry Department, College of Science, King Saud University, Riyadh 11451, Saudi Arabia. rbhat@ksu.edu.sa (R.B).
*Correspondence: hrizwana@ksu.edu.sa.

Abstract

Phytopathogens cause considerable postharvest losses in fruits and vegetables. Although chemical fungicides are widely used for their control, their toxic effects on living organisms and the environment cannot be ignored. Therefore, this study explored a plant-based approach by synthesizing silver nanoparticles (AgNPs) from banana flowers (Bf) grown in Jazan, Saudi Arabia. The synthesized Bf-AgNPs were investigated for their antifungal, antioxidant, and cytotoxic potential. GC-MS analysis was performed to investigate the phytochemical composition of banana flower extract, followed by preliminary molecular docking of selected compounds. The synthesized Bf-AgNPs were characterized using UV-Vis, TEM, DLS, FTIR, XRD, and EDX. UV-Vis spectroscopy showed an absorption band at ~422 nm. TEM analysis showed an average NP size of 18.96 nm, while DLS revealed a hydrodynamic size of 87.42 nm with a PDI of 0.28. The Bf-AgNPs showed notable inhibition of mycelial growth and spore germination at 50 µg/mL for most tested pathogens, except *Pestalotiopsis mangiferae*. The MIC and MFC values for susceptible isolates ranged from 25 to 100 µg/mL and 50 to >200 µg/mL, respectively, whereas *P. mangiferae* exhibited an MIC of >200 µg/mL. Scanning electron microscopy of treated fungal pathogens revealed pronounced structural changes. Furthermore, the Bf-AgNPs exhibited significant, dose-dependent antioxidant activity and cytotoxicity against the A549 and HEp-2 cancer cell lines. Preliminary molecular docking of the selected phytochemicals against sterol 14α-demethylase (CYP51B) showed binding affinity scores ranging from −5.8 to −6.3 kcal/mol, suggesting possible interaction with the target protein. To the best of our knowledge, previous studies have not explored the antifungal activity of silver nanoparticles synthesized from banana flowers grown in Saudi Arabia against the postharvest pathogens tested in the present study. The results indicate that banana flower-mediated silver nanoparticles show promising in vitro inhibitory activity against selected postharvest pathogens; however, their efficacy and safety warrant further evaluation under postharvest conditions to establish their practical applicability.

Keywords: Banana flowers, Saudi Arabia, postharvest fungi, AgNPs, sunlight, antifungal, cytotoxic, molecular docking.

1. Introduction

The banana plant is an herbaceous, monocot perennial in the family Musaceae and genus Musa [1]. Bananas are among the most widely consumed, produced, and traded fruits globally and are primarily cultivated in tropical and subtropical countries [2]. In recent years, the global banana trade has reached approximately 20 million tons annually [2]. Bananas are a good source of important nutrients, which contribute to their health benefits and economic importance [3,4]. The world's leading banana producers include India, China, Indonesia, the Philippines, Brazil, and Ecuador [5], reflecting the global demand for this crop. Recently, Saudi Arabia has introduced some Musa species in the Jazan province, including *Musa acuminata* and *Musa paradisiaca* [6].

In recent years, global demand has driven a rise in banana production; however, very little attention has been paid to its by-products [1]. During harvest, banana plantations produce considerable quantities of by-products such as stalks, leaves, inflorescence, and stems, yet most remain underutilized [6,7]. These by-products can be used across sectors to produce value-added products, creating opportunities for sustainable resource use. The banana inflorescence, often called the banana blossom, is a purplish or reddish, multilayered, pendulous structure with colourful bracts that bear and protect the flowers in whorls. The tender bracts and the flowers are edible and are consumed fried, in soups, and in curries in many Asian countries [8,9].

The inflorescence of different banana cultivars contains a diverse array of vitamins, amino acids, proteins, dietary fibre, fatty acids, macro and microelements, and bioactive phytochemicals like phenols and flavonoids, steroids, and anthocyanins, which collectively contribute to their nutritional, medicinal, and therapeutic value [9,10,11,12]. In Folk medicine, banana flowers are used to treat diabetes mellitus, diarrhoea, gastric issues, asthma, dysmenorrhea [13], and to increase lactation in postpartum mothers [14]. Previous studies have demonstrated the anticancer [15,16,17], antioxidant and anti-diabetic properties [17,18,19] of banana flowers and bracts.

Among all microorganisms, fungal pathogens contribute heavily to postharvest losses worldwide [20]. Postharvest losses of fruits and vegetables primarily result from their high moisture content, which makes them highly perishable and vulnerable to rot and spoilage [21,22]. Infection may begin before harvest, during harvest, or at any stage of postharvest operations, such as handling, transport or storage [22]. Some infections are latent: the pathogen remains quiescent, and once conditions become favourable, symptoms develop rapidly, leading to decay and deterioration [20,22]. The deterioration reduces the shelf life, affecting the market value of fresh produce (fruits and vegetables, causing food security issues and incurring major economic losses across the supply chain [23,24]. The FAO reported that global postharvest losses for fruit and vegetables increased from 23.2% in 2015 to 25.4% in 2023 [25].

Worldwide, chemical fungicides are used indiscriminately or overused to control fungal pathogens that cause postharvest losses; although they are effective, the environmental hazards they pose cannot be ignored and remain a major concern. Although recent advances in technology have provided the agricultural sector with highly sensitive materials capable of early detection of diseases or pathogen presence in fruits/vegetables, these sophisticated innovations are yet to be tested and validated on a large scale [26]. Therefore, there is a pressing need for

alternative disease management strategies that not only improve crop quality and extend shelf life but are also sustainable and eco-friendly to strengthen the global agricultural economy.

Given the huge postharvest losses incurred every year, innovative approaches are essential to combat fungal growth, and nanobiotechnology ranks among the most promising tools currently in use in agricultural practices. Green synthesized silver nanoparticles from different plant parts, including leaves [27,28], fruits [29], seeds [30,31,32], and flowers [33], have consistently demonstrated strong antifungal activity in earlier reports [27-33].

Considering the varied health, therapeutic and nutritional benefits of banana inflorescence, and the burgeoning demand for ecologically safe antifungal agents to mitigate postharvest losses caused by fungal pathogens, our study explored the antifungal efficacy of green synthesized silver nanoparticles (AgNPs) derived from the banana flowers against some key phytopathogenic fungi responsible for causing soft rots of fruits and vegetables. This study is novel because, to our knowledge, it is the first to explore banana flowers grown in Saudi Arabia for their antifungal activity against important postharvest pathogens, as well as for other biological activities.

2. Materials and Methods

2.1 Chemical compounds, Plant material

The culture media, chemical compounds, and reagents used in this study were of standard analytical grade (99% pure) and were purchased from Sigma-Aldrich (Saint Louis, MO, USA). The plant material used was *Musa acuminata* flowers.

2.2 Synthesis of silver nanoparticles (AgNPs) using aqueous extract of banana flower (Bf).

Fresh, healthy banana inflorescences of *Musa acuminata* cv. Grand Nain were collected from a local farm in Jazan province, Saudi Arabia. A qualified taxonomist in the Department of Botany, King Saud University, Riyadh, Saudi Arabia, authenticated the plant material. After authentication, the inflorescence was washed, the colorful bracts were carefully removed, and the flowers were separated. The flowers were thoroughly washed, air-dried at room temperature, and then finely ground in a mechanical grinder [23]. Approximately 20 g of Bf powder was dissolved in 200 mL of sterilized distilled water and heated at 60 °C for 20 minutes. After cooling, the mixture was filtered, and the resulting filtrate (Bf aqueous extract) was centrifuged at 5000 rpm. The supernatant was used in subsequent experiments. Bf-AgNPs were synthesized under direct sunlight. The reaction mixture, comprising 90 mL of aqueous silver nitrate (1 mM) and 10 mL of Bf aqueous extract, was prepared in a glass flask. The flask was placed under natural sunlight and shaken at regular intervals to ensure uniform mixing. Nanoparticle formation was observed visually as the mustard-yellow colour of the reaction mixture changed to brown, indicating successful NP synthesis. The reaction mixture was centrifuged at 9,000 rpm for 30 minutes and washed with distilled water to remove residual impurities. This purification step was repeated three times to ensure complete removal of unreacted components. The purified Bf-AgNPs were then stored at 4 °C for subsequent characterization and biological assays.

2.3 Characterization of Bf-AgNPs

The absorption spectrum of Bf-AgNPs was obtained using a UV–Vis spectrophotometer (Shimadzu Model 1800, Kyoto, Japan). The size and morphology of the purified Bf-AgNPs were examined using transmission electron microscopy (TEM, JEOL(JEM-Plus 1400), Tokyo, Japan). The average nanoparticle size was determined by measuring 100 nanoparticles, and a histogram was generated using Origin Pro (2027). A small aliquot of the sample was mounted on a carbon-coated copper grid and imaged at an accelerating voltage of 100 kV to obtain high-resolution TEM micrographs. The crystalline structure of the NPs was verified with an X-ray diffractometer (PANalytical, San Francisco, CA, USA), which operated at 40 kV and 30 mA and scanned across the 2θ range to identify characteristic diffraction peaks. Fourier transform infrared (FTIR) spectroscopy (Shimadzu, USA; 400–4000 cm^{-1}) was used to identify functional groups involved in nanoparticle formation. The FTIR spectra of the Bf extract and the Bf-AgNPs were recorded using a Thermo Scientific FTIR Model 6700 (Waltham, Massachusetts, USA) with the KBr pellet method at a resolution of 4 cm^{-1}. A Zetasizer Ultra ZSU-3305 (Malvern Instruments, UK) was used to determine the average hydrodynamic size of the nanoparticles. Elemental composition was examined with energy-dispersive X-ray spectroscopy (EDS) at 30 kV, coupled with a JEOL scanning electron microscope (FESEM-EDAX; JSM-7610F, Japan). All characterization procedures were performed according to the respective instrument manufacturers' guidelines.

2.4 Postharvest fungal pathogens

The following phytopathogens responsible for postharvest rots such as *Alternaria alternata f. sp. lycopersici, Alternaria tenuissima, Fusarium oxysporum, Fusarium solani, Helminthosporium solani, Pestalotiopsis mangiferae*, and *Colletotrichum musae* were procured from the College of Food and Agricultural Sciences, Department of Plant Protection, and Department of Botany and Microbiology, King Saud University, Riyadh, Saudi Arabia.

2.5 Antifungal activity of Bf-AgNPs against postharvest fungal pathogens

The inhibitory activity of Bf-AgNPs on selected postharvest pathogens was determined using the method described in an earlier study [34]. Pure fungal cultures of *Alternaria alternata f. sp. Lycopersici, Alternaria tenuissima, Fusarium oxysporum, Fusarium solani, Helminthosporium solani, Pestalotiopsis magnifera*, and *Colletotrichum musae* were subcultured and grown for 7 days on Potato dextrose agar (PDA), and these freshly grown cultures were used for the antifungal assay. Sterilized PDA was amended separately with Bf-AgNPs (50 µg/mL), Bf-aqueous flower extract (50 µg/mL), $AgNO_3$ (0.1 mM) and tebuconazole (25µg/mL). The test concentration for initial screening was determined based on a previous study. Each treated medium was dispensed into sterile petri plates separately and allowed to solidify at 25–26 °C. The antifungal activity of these treatments was assessed by placing a 6 mm mycelial disc of the test fungal pathogens in the center of amended PDA plates, with the colony surface touching the PDA medium (upside down) to ensure direct contact with the medium. The fungal plug (6 mm) was excised aseptically from the actively growing edge of a pure 7-day-old fungal culture plate. PDA supplemented with tebuconazole served as the positive control, whereas untreated PDA plates functioned as the negative control. The mycelial growth of both the treated and untreated fungi was measured, and their corresponding percentage inhibition was calculated [27]. Each fungal isolate was evaluated in a similar manner, with every treatment repeated three times.

2.6 Effect of Bf-AgNPs on the Spore Germination of Selected Post-Harvest Fungal Pathogens

The inhibitory potential of Bf-AgNPs (50 µg/mL) and the fungicide (25 µg/mL) on spore germination of the selected pathogens was evaluated in potato dextrose broth, as described earlier, with a minor modification [35]. Spore suspensions of test isolates were prepared as described by Rizwana et al. [34]. Briefly, equal volumes (500 µL) of Bf-AgNPs and fungal spore suspension (1×10^6 spores/mL) were transferred to a 1 mL sterile test tube to achieve final concentrations. A test tube containing spore suspension in sterilized distilled water served as the negative control, while fungicide served as the positive control. All test tubes were incubated in the dark at 28°C for 24 h. After 24 h of incubation, the spore germination rate was observed under the microscope, and the observations were recorded. A small aliquot from each treatment and control was stained with lactophenol cotton blue on a clean slide and examined under a light microscope. Percentage germination inhibition was quantified by counting 100 spores per treatment and control [36,37]. The assay was conducted three times for each fungal isolate.

2.7 Scanning electron microscopy observations of Bf-AgNP induced morphological changes.

SEM was used to observe Bf-AgNP-induced morphological deformities in fungal isolates and compare them with untreated fungal samples. Fungal isolates exhibiting potent growth inhibition at their MIC concentrations were selected for SEM imaging. Fungal mycelial discs were aseptically removed from selected isolates and centrifuged (8000 rpm, 5 min). The resulting pellets were fixed in 2.5% glutaraldehyde for 48 h, washed three times with Tris–acetate buffer (0.1 mol/L, pH 7.2), and then dehydrated through a graded ethanol series (60–100%). The specimens were freeze-dried (critical point dryer), mounted on gold-coated stubs, and examined. Micrographs were captured using SEM-JSM-6060LV (JEOL, Japan Ltd.).

2.8 Cytotoxicity assay and Cell line Culture

In this study, two cancer cell lines, namely the A549 lung carcinoma cell line (ATCC CCL-185) and the HEp-2 cell line (a HeLa derivative; ATCC CCL-23), obtained from the American Type Culture Collection (ATCC), were screened for their response to Bf-AgNPS. Dulbecco's Modified Eagle Medium (DMEM; 4.5 g/L glucose, L-glutamine) and foetal bovine serum (FBS) were obtained from Gibco, Invitrogen (Grand Island, NY, USA). Penicillin–streptomycin and MTT reagent [3-(4,5-dimethylthiazol-2-yl)-2,5-diphenyltetrazolium bromide] were purchased from Sigma-Aldrich Ltd. (Ayrshire, UK).

2.8.1 Cell Culture: HEp-2 and A549 cell lines were maintained in Dulbecco's Modified Eagle Medium (DMEM) supplemented with 10% fetal bovine serum (FBS) and 1% penicillin–streptomycin. Cultures were incubated at 37 °C (24 h) and grown until a confluent monolayer (70–90%) was established. For routine maintenance, cells were washed twice with phosphate buffered saline (PBS) and detached using 1.0 mL of 25% trypsin containing 0.53 mM EDTA. The harvested cells were transferred to 25 cm^2 culture flasks and incubated overnight in a humidified atmosphere (37 °C, 5% CO_2, 95% air). Subcultured at least once per week to ensure optimal growth conditions [38].

2.8.2 MTT assay: The cytotoxic activity of the banana aqueous extract and Bf-AgNPs against HEp-2 and A549 cells was evaluated using the MTT assay (3-[4,5-dimethylthiazole-2-yl]-2,5-diphenyltetrazolium bromide). Exponentially growing cells were detached with 0.25% trypsin–EDTA and seeded into 96-well plates at 1×10^4 cells/well in 100 µL of complete medium. After a 24-h stabilization period, cells were exposed to increasing concentrations of the extract and AgNPs (50, 100, 200, and 400 µg/mL). Treatments were prepared in DMEM containing FBS and 1% penicillin–streptomycin, and plates were incubated for 24 h at 37 °C in a humidified 5% CO_2 environment. Doxorubicin served as the positive control. Following treatment, 10 µL of MTT working solution (5 mg/mL in PBS) was added to each well and incubated for 4 h at 37 °C. The resulting formazan crystals were solubilised with 100 µL of DMSO per well and gently shaken for 10 min at 37 °C. Absorbance was recorded at 590 nm using an ELX-808 microplate reader (BioTek Laboratories, Shoreline, WA, USA), and cytotoxicity (%) was calculated [39]. We determined the inhibitory concentration (IC_{50}) using GraphPad Prism.

2.9. DPPH Scavenging Assay

The antioxidant potential of the Bf-AgNPs was assessed using the DPPH free radical scavenging assay (2,2-diphenyl-1-picrylhydrazyl, DPPH) with minor modifications [40]. Briefly, a 0.1 mM DPPH solution was prepared in methanol. Different concentrations of AgNPs (50, 100, 200, 300, 400 and 500 µg mL^{-1}) were mixed with the DPPH solution (0.1 mM) and incubated in the dark at 37°C for 30 min. Following incubation, the absorbance of each reaction mixture was measured at 517 nm using a UV-Vis spectrophotometer. The assay was run with ascorbic acid as a reference control at concentrations of 50, 100, 200, 300, 400, and 500 µg mL^{-1}, similar to Bf-AgNPs, while the blank was DPPH solution alone. The radical scavenging activity was expressed as percentage inhibition and calculated using the following equation. The IC50 value for both Bf-AgNPs and ascorbic acid was determined from dose-response curves using linear regression analysis. The results are the means of three independent experiments.

Scavenging activity (%) = [(Ac-As/Ac)]/100

where Ac represents the absorbance of the control (without test sample) and As represents the absorbance of the sample.

2.10. GC-MS analysis

The chemical composition of the methanolic extract of banana flowers was analysed using a gas chromatography-mass spectrometry (GC-MS) system (Agilent 7890A) coupled to a mass spectrometer (5975C; Agilent Technologies, Santa Clara, CA, USA). The instrument was fitted with a DB-5MS capillary column (30 m × 0.25 mm i.d., 0.25 µm film thickness), a Triple-Axis detector, and an automatic liquid sampler. Before analysis, the extract was filtered through a 0.22 µm membrane filter, and 1 µL of the filtrate was injected into the system. The injector and column temperatures were set at 280°C and 300°C, respectively. Helium served as the carrier gas at 1 mL/min, and mass spectra were acquired using electron ionisation at 70 eV. Compound identification was achieved by comparing the spectra with those in standard spectral databases archived in the NIST/EPA/NIH Mass Spectral Library (NIST 14, 2014 edition), which is incorporated into the GC-MS analysis software. The instrument was operated in accordance with the manufacturer's instructions.

2.11. Docking Analysis

The crystal structure of sterol 14α-demethylase (CYP51B) was obtained from the Protein Data Bank (https://www.rcsb.org/; PDB ID: 4UYM). The structures of the seven selected compounds were retrieved from PubChem using the compound identifiers listed in Table 1. Protein–ligand docking was performed using CB-Dock, a web server that integrates cavity detection with AutoDock Vina [-41,42]. Each compound was submitted separately with the receptor structure, and docking was performed within five predicted cavities. The resulting poses were ranked by Vina score, and the pose with the most negative score was selected for visualization.

3. Results

3.1 Formation of Bf-AgNPs

Bf-AgNP formation was indicated when the mustard-yellow aqueous extract of banana flowers changed to brown upon addition of 1 mM AgNO3 solution and direct exposure to sunlight. Under direct sunlight, the nanosynthesis process was rapid, with brown colour formation occurring in about 17 minutes, indicating Bf-AgNP formation (Figure 1). UV–Vis spectroscopy corroborated Bf-AgNP formation, and a broad peak at 422 nm in the UV spectrum, corresponding to surface plasmon resonance, further confirmed Bf-AgNP formation (Figure 2). The 278 nm peak reflects polyphenols that helped reduce and cap the AgNPs and remained on their surface as stabilizing residues.

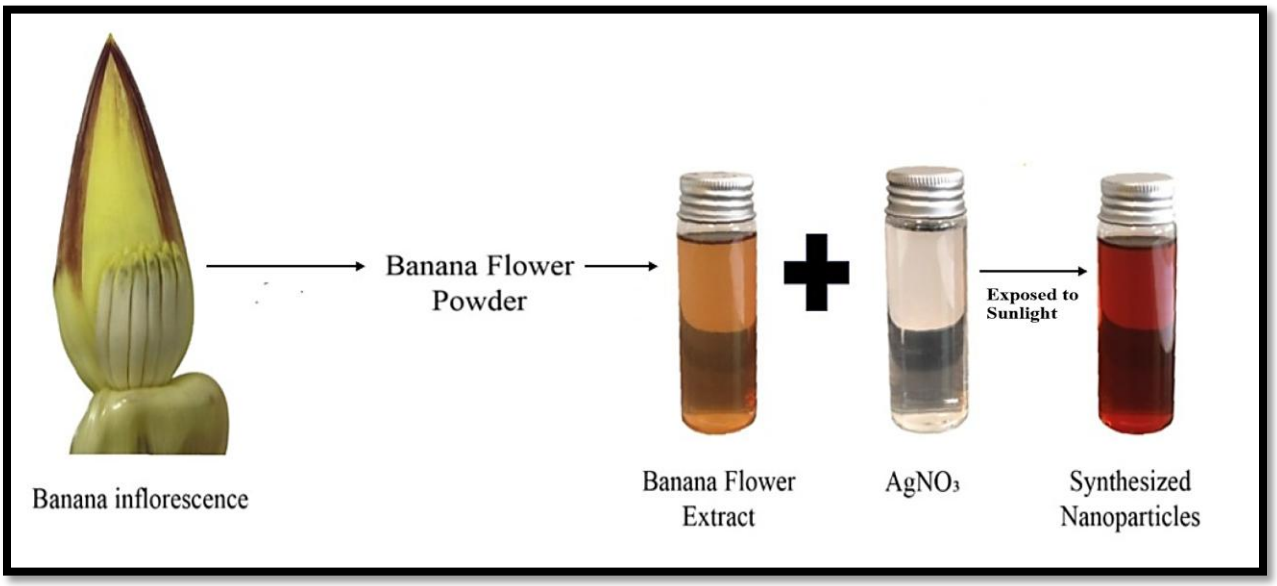


Figure 1. Sunlight-mediated nanoparticle formation from aqueous extract of banana flowers.

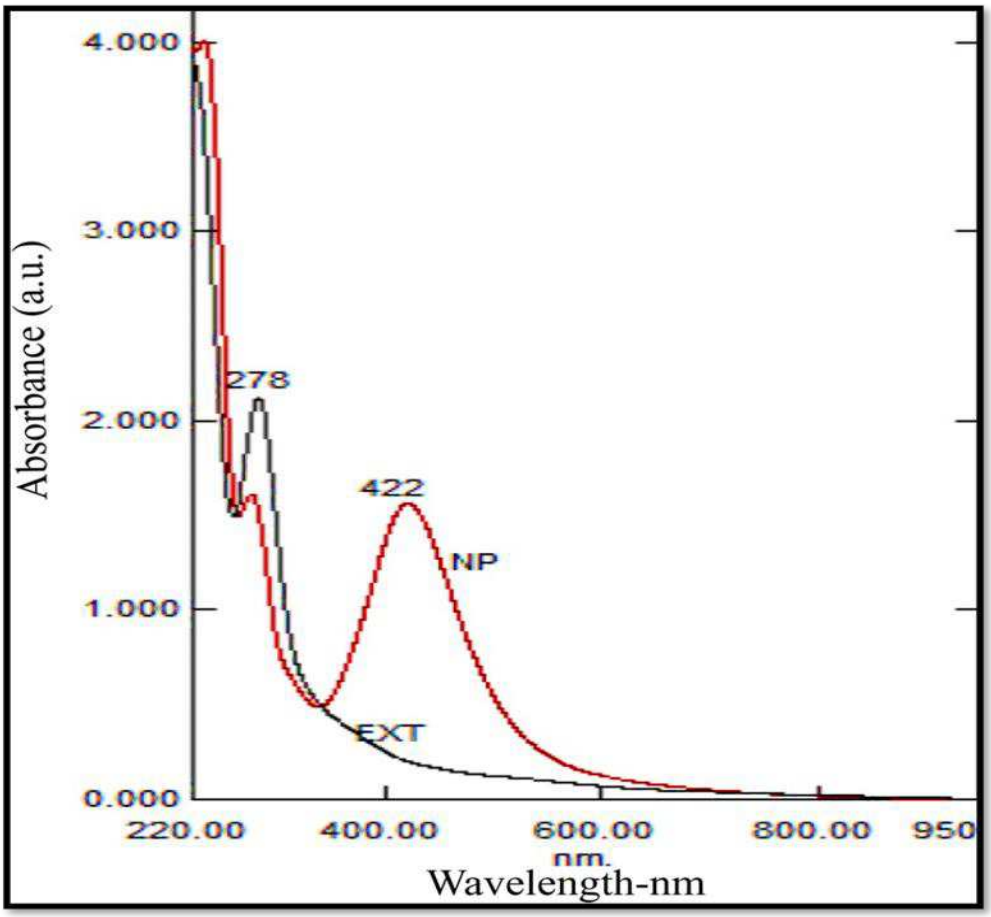
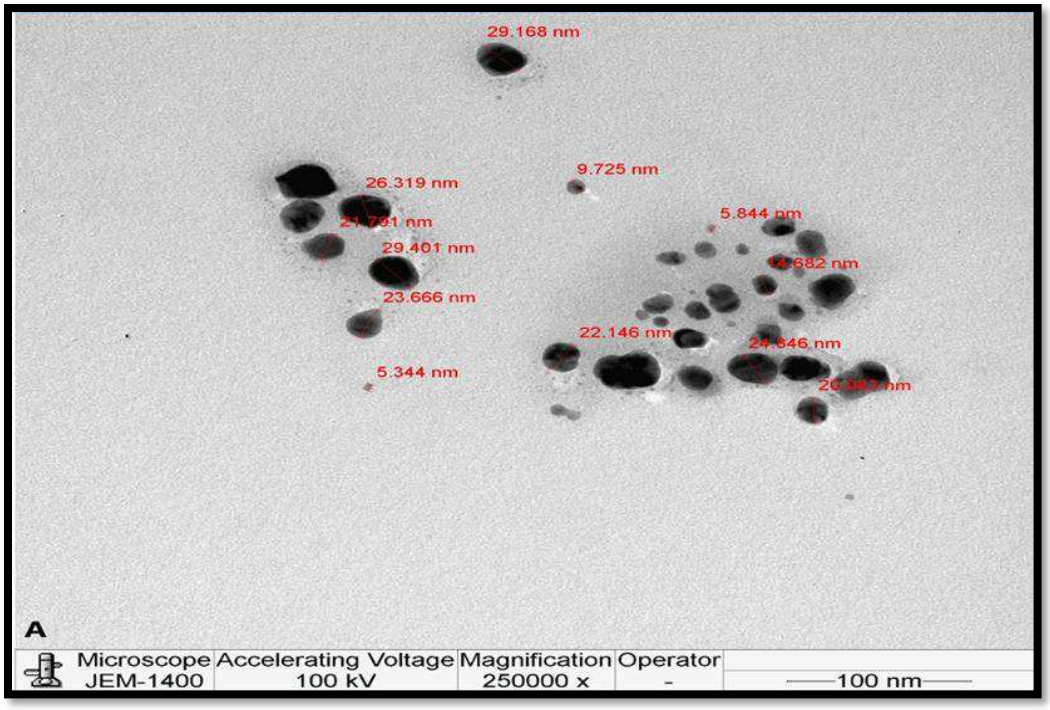


Figure 2. UV-Vis spectrum of Bf-AgNPs prepared from banana flower extract (black line) and banana flower silver nanoparticles (Bf-AgNPs, red line).

3.2 Characterization of Bf-AgNPs

3.2.1 Size and Morphology of Bf-AgNPs

The morphology, shape and size of Bf-AgNPs were observed by TEM (Transmission Electron Microscopy). The TEM microphotograph shown below indicates that the nanoparticles were uniformly dispersed and predominantly spherical to quasi-spherical, with sizes ranging from 5.34 nm to 29. 401 nm and an average size of 18.96 nm (Figure 3A, B). Dynamic light scattering (DLS) further showed an average hydrodynamic diameter of 87.42 nm with a polydispersity index (PDI) of 0.28 (Figure 4).



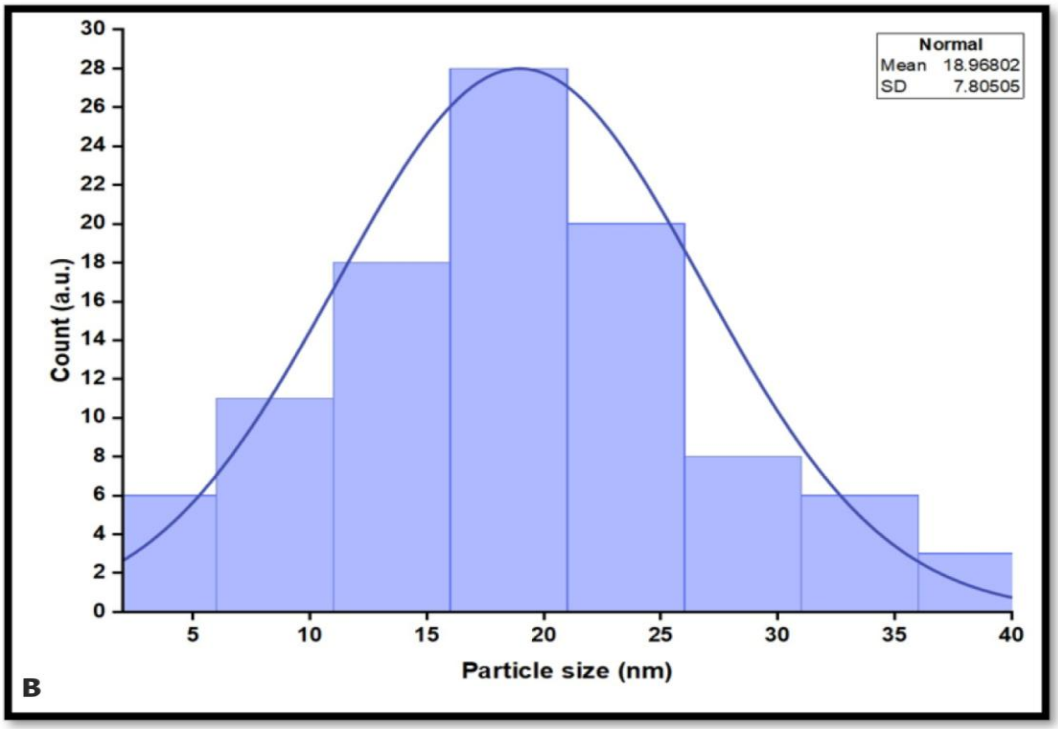


Figure 3.**A)** TEM micrograph showing the size and morphology of Bf-AgNPs. **(B)** Histogram of the size distribution of Bf-AgNPs based on TEM images.

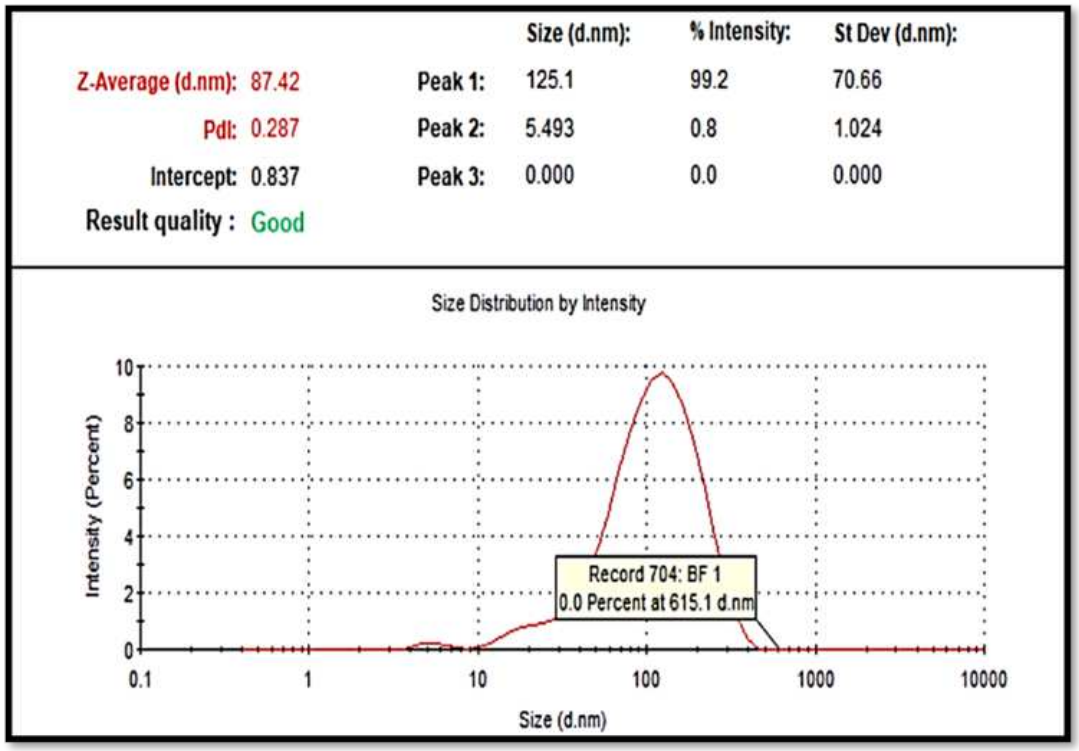


Figure 4. Dynamic light scattering spectrum illustrating the hydrodynamic size (Z average) of the Bf-AgNPs.

3.2.2 Functional Groups in the extract and Bf-AgNPs

Banana flower extract and Bf-AgNPs were subjected to FTIR analysis (400–4000 cm^{-1}) in order to identify the functional groups responsible for capping and stabilisation of the Bf-AgNPs (Figure 5). The spectra of both the Bf-extract and Bf-AgNPs showed strong peaks attributable to phenolics, flavonoids, hydroxyl, carbonyl, and amine groups. The Bf-extract spectrum showed a broad absorption band at 3399 cm^{-1}, corresponding to O–H stretching in phenolic and flavonoid groups, while peaks at 2926 and 2856 cm^{-1} corresponded to aliphatic C–H stretching. The band at 1712 cm^{-1} was due to the C=O stretching of organic acids and esters, and the peak at 1620 cm^{-1} was due to amide I or aromatic C=C stretching, indicating the presence of proteins and aromatic compounds. In addition, peaks between 1457 and 1054 cm^{-1} were attributed to C–H bending and C–O stretching of polysaccharides and phenolic derivatives. After nanoparticle formation, the FTIR spectrum of BF-AgNPs showed peaks at 3399, 2928, 1721, 1635, 1419, 1255, 1059, 917, 867, 818, 777, and 590 cm^{-1}, which were quite similar to the extract spectrum. However, some peaks shifted to new positions, such as 1721 and 1635 cm^{-1}. Besides, two new peaks appeared in the Bf-AgNP spectrum at 1255 and 917 cm^{-1}, and the distinct peak at 590 cm^{-1} arose due to Ag–O or metal biomolecule vibrations and confirms the formation of the nanoparticles and their capping.

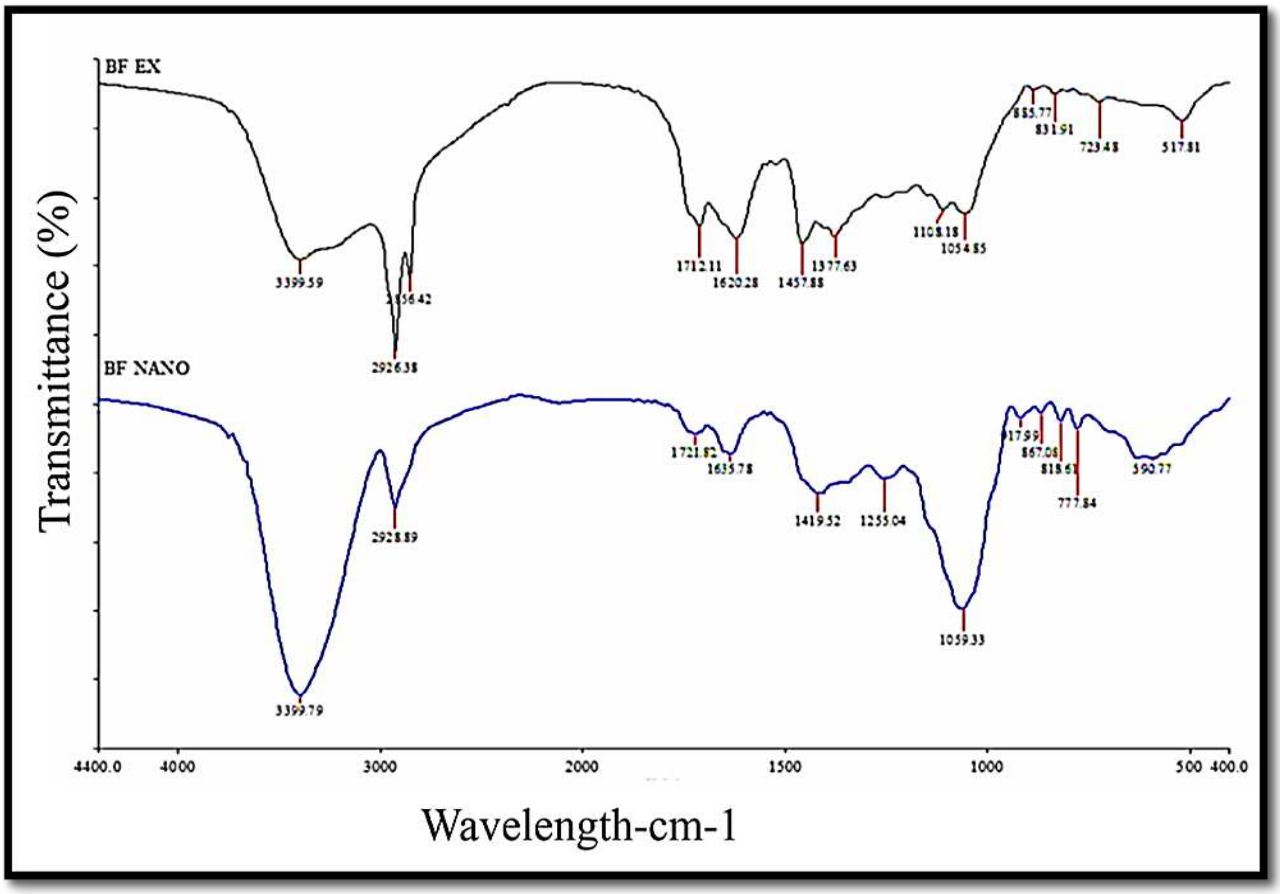


Figure 5. FTIR spectral profiles of functional groups present in banana extract (BF-EX) and banana silver nanoparticles (Bf-AgNPs).

3.2.3 Crystalline structure and elemental composition of Bf-AgNPs

The XRD pattern (2θ range) shown in Figure 6 shows diffraction peaks corresponding to the (101), (111), (200), (220), and (311) planes, indicating the characteristic face-centred cubic (fcc) structure of metallic silver. The pattern is in agreement with the standard JCPDS reference data for Ag^0 (JCPDS file no. 04-0783). The EDS spectrum showed a dominant silver signal (Ag-36.05%) at 3 keV and 2.6 keV, which confirms that silver is the major constituent. The spectrum also showed signals for C (26.84%), O (33.52%), Na (0.67%), Cl (0.48%), K (2.11%) and Ca (0.32%) (Figure 7A, B).

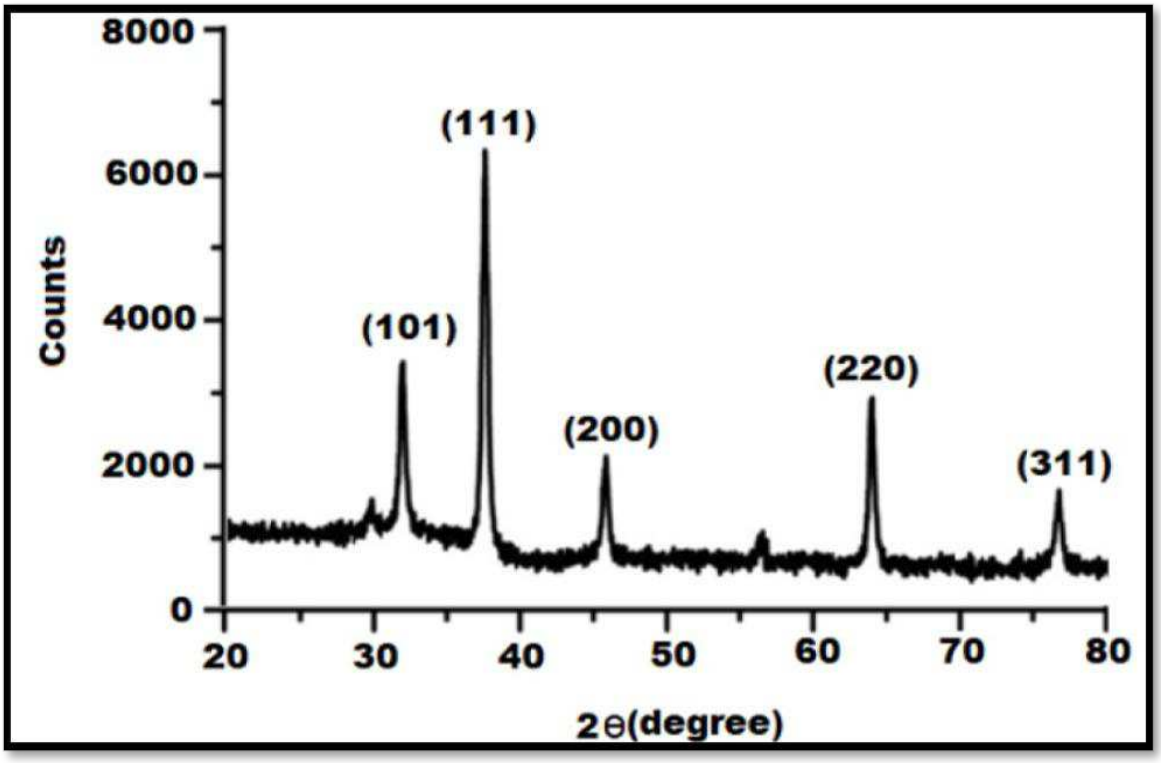
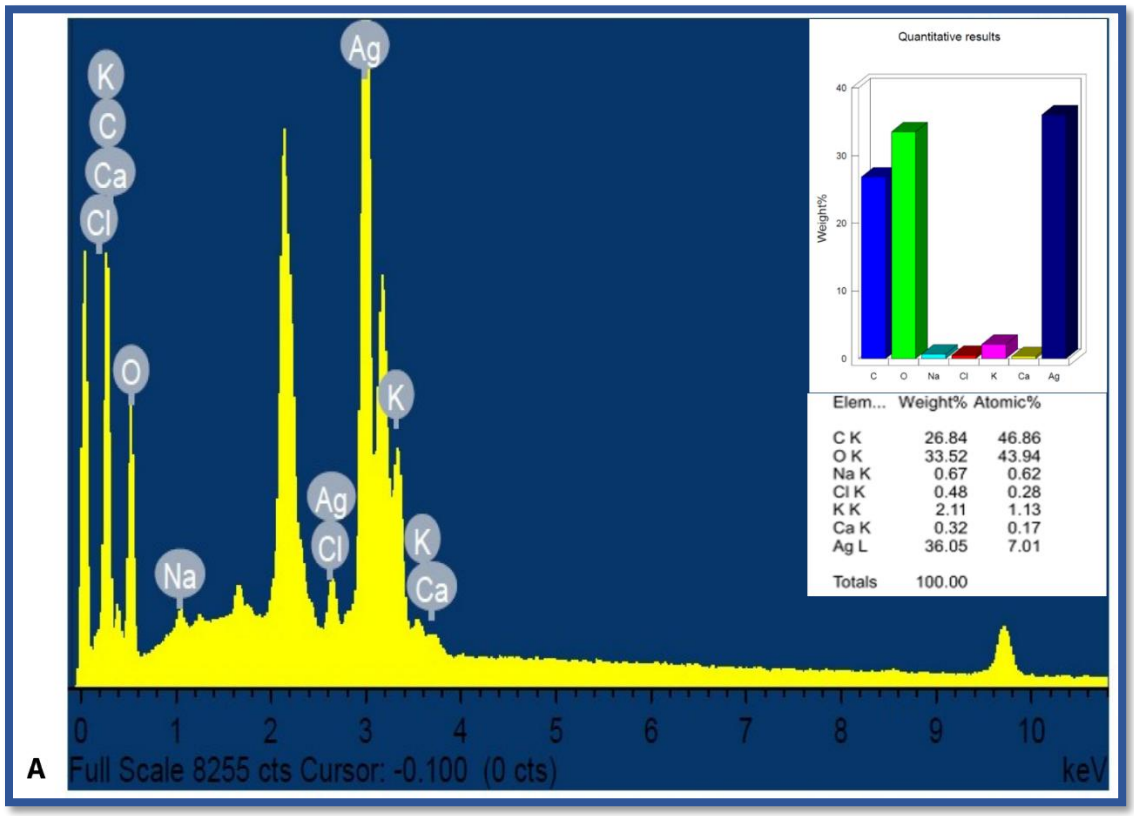


Figure 6. X-ray diffraction pattern of Bf-AgNPs



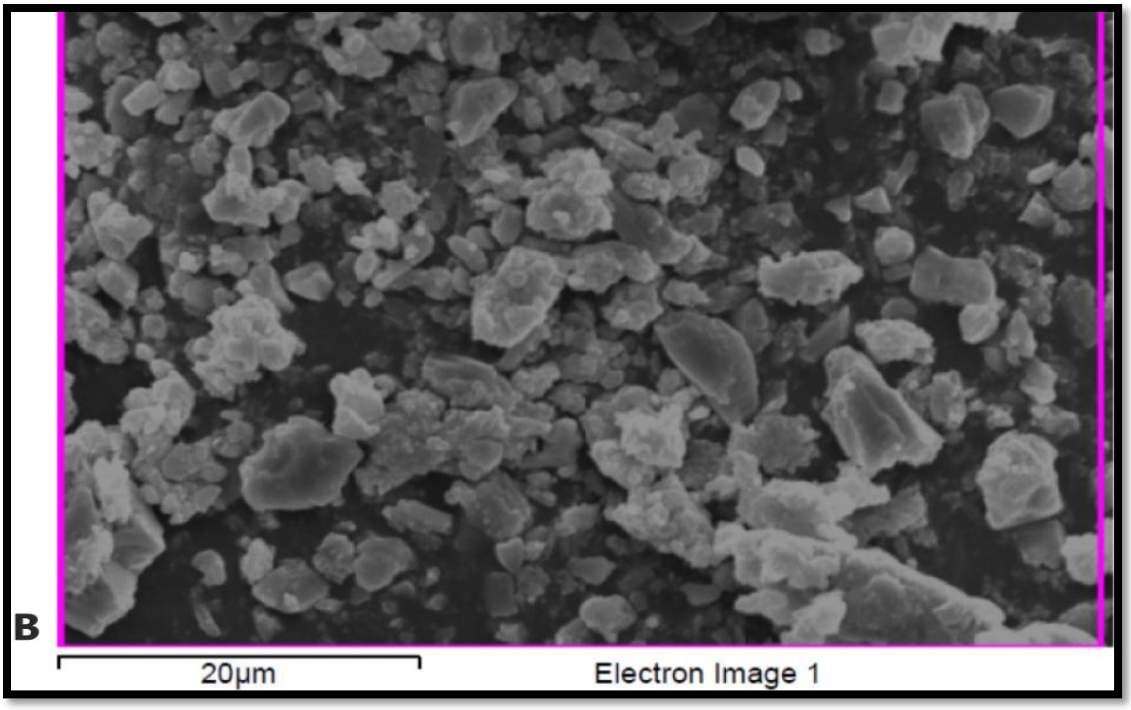


Figure 7A. EDX spectrum illustrating the elemental profile of Bf-AgNPs; **B-**SEM microphotographs of Bf-AgNPs

3.3 Antifungal activity of Bf-AgNPs on inhibition of mycelial growth and MIC concentrations

The silver nanoparticles synthesized from banana flowers (Bf-AgNPs) exhibited inhibitory effects ($p \leq 0.05$) against all postharvest fungal pathogens tested in this study, except *Pestalotiopsis mangiferae*, which showed no measurable inhibition at the test concentration (50 µg/mL) (Figure 8). The figure related to in vitro studies has been reported as Supplementary Figure 1; Bf-AgNps at 50 µg/mL completely inhibited the mycelial growth of *Alternaria alternata*, closely comparable to the inhibition caused by the fungicide tebuconazole, followed sequentially by *Fusarium solani*, *F. oxysporum*, *Colletotrichum musae*, and *Alternaria tenuissima*. Correspondingly, Figure 9 shows the percentage mycelial growth inhibition of fungal pathogens: *A. alternata* (100%), *H. solani* (83%), *F. solani* (74%), *C. musa*e (67%), *F. oxysporum* (55%) and *A. tenuissima* (50%). The chemical fungicide tebuconazole, used as a positive control, significantly inhibited all the tested fungal pathogens ($p \leq 0.05$), as seen in Figures 8 and 9. The MIC of Bf-AgNPs ranged from 25 µg/mL to 200 µg/mL, while the MFC ranged from 50 µg/mL to >200 µg/mL (Table 1)

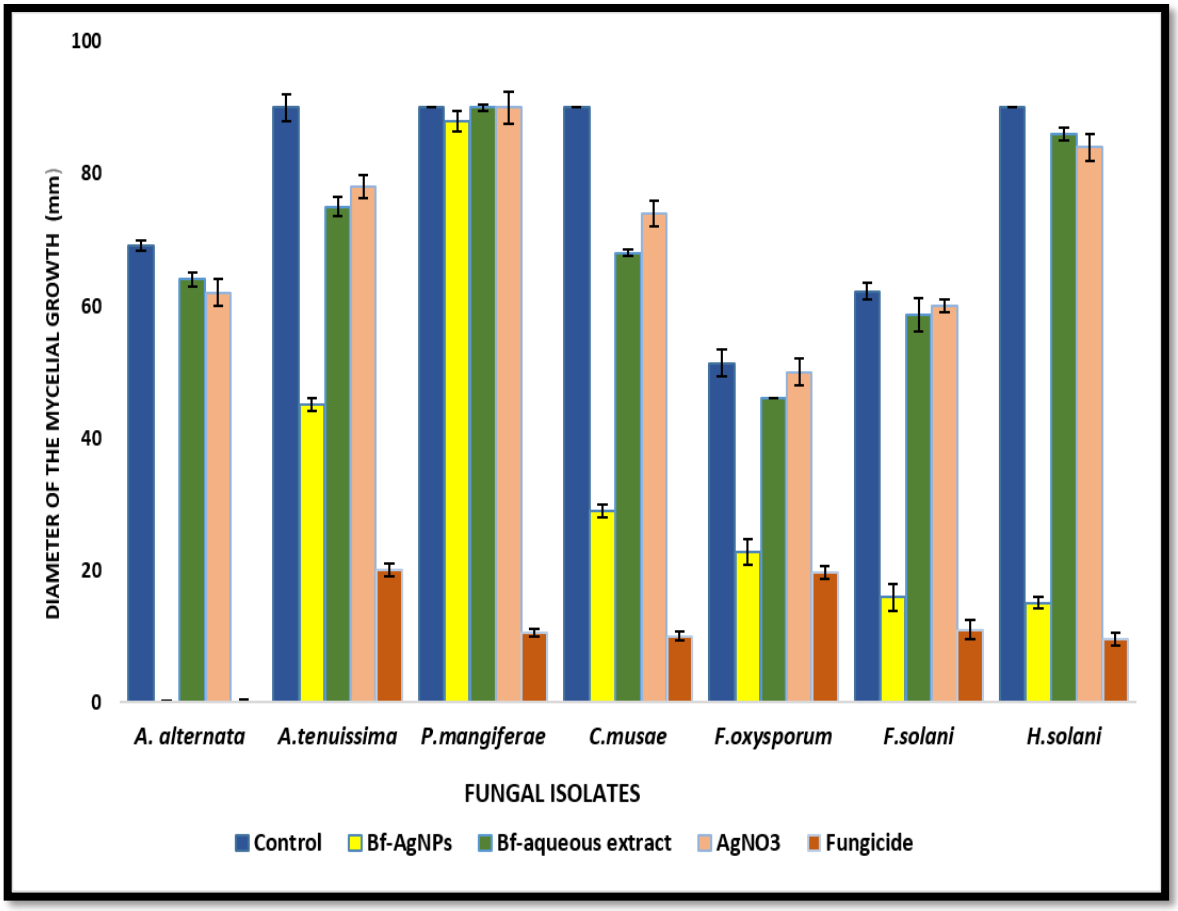


Figure 8. Effect of Bf-AgNPs (banana silver nanoparticles); Banana (aq) extract; $AgN0_3$ and fungicide tebuconazole on the mycelial growth of test pathogens. *A. alternata* (*Alternaria alternata f. sp. Lycopersici*); *A. tenuissima* (*Alternaria tenuissima*); *P.mangiferae* (*Pestalotiopsis mangiferae*) *C. musae* (*Colletotrichum musae*); *F.oxysporum* (*Fusarium oxysporum*); *F. solani* (*Fusarium solani*); *H. solani* (*Helminthosporium solani*). The values shown in the graph are means of three independent experimental replicates (±SD). Significant differences among treatments were assessed using one-way ANOVA followed by Tukey's HSD test ($p \leq 0.05$).

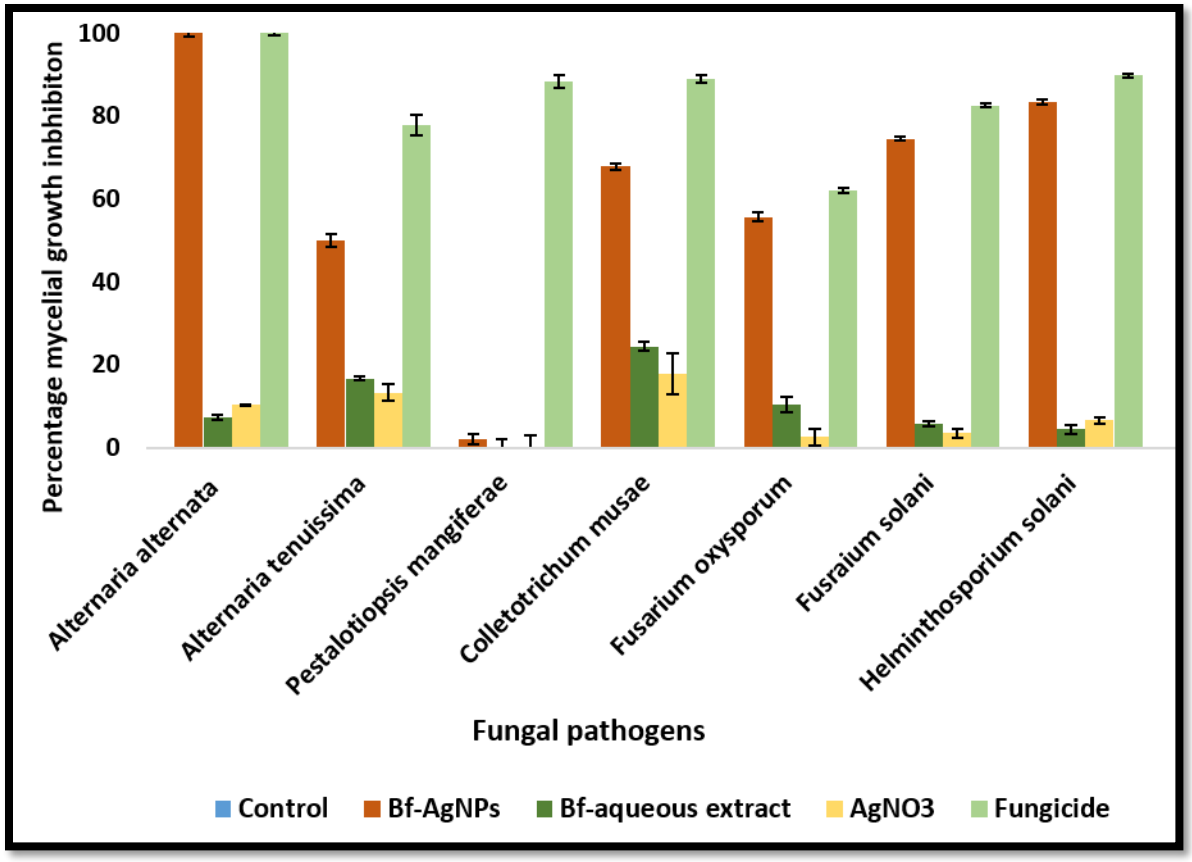


Figure 9. Percentage mycelial growth inhibition of fungal test pathogens treated with Bf-AgNPs, Bf-extract, AgNO3, and tebuconazole. Data represent the mean of three replicates (±SD). Differences among treatments were assessed using one way ANOVA followed by Tukey's HSD test ($p \leq 0.05$).

Table 1. Minimum inhibitory concentration (MIC) and minimum fungicidal concentration (MFC) of synthesized banana flower silver nanoparticles (Bf-AgNPs) and the fungicide (tebuconazole)

Fungal pathogens	Bf-AgNPs (µg/mL)		Fungicide (µg/mL)	
	MIC	MFC	MIC	MFC
Alternaria alternata f. sp. lycopersici	25	50	12.5	25
Alternarai tenuissima	100	200	50	100
Pestalotiopsis mangiferae	>200	NT	25	100
Colletotrichum musae	100	100	25	50
Fusarium oxysporum	100	>200	50	100
Fusraium solani	100	200	50	100
Helminthosporium solani	100	100	50	50

3.4 Inhibition of Spore Germination

The in vitro assay evaluating the effect of BF AgNPs on spore germination showed a clear concentration-dependent inhibition across all tested pathogens (Figure 10). The number of spores germinated (%) at 50 µg/mL was as follows: 0%,48%, 95%,38%,45%, 20% and 25% for *A.alternata, A.tenuissima, P. mangiferae*, *C.musae, F. oxysporum*, *F. solani* and *H. solani,* respectively (Figure 10).

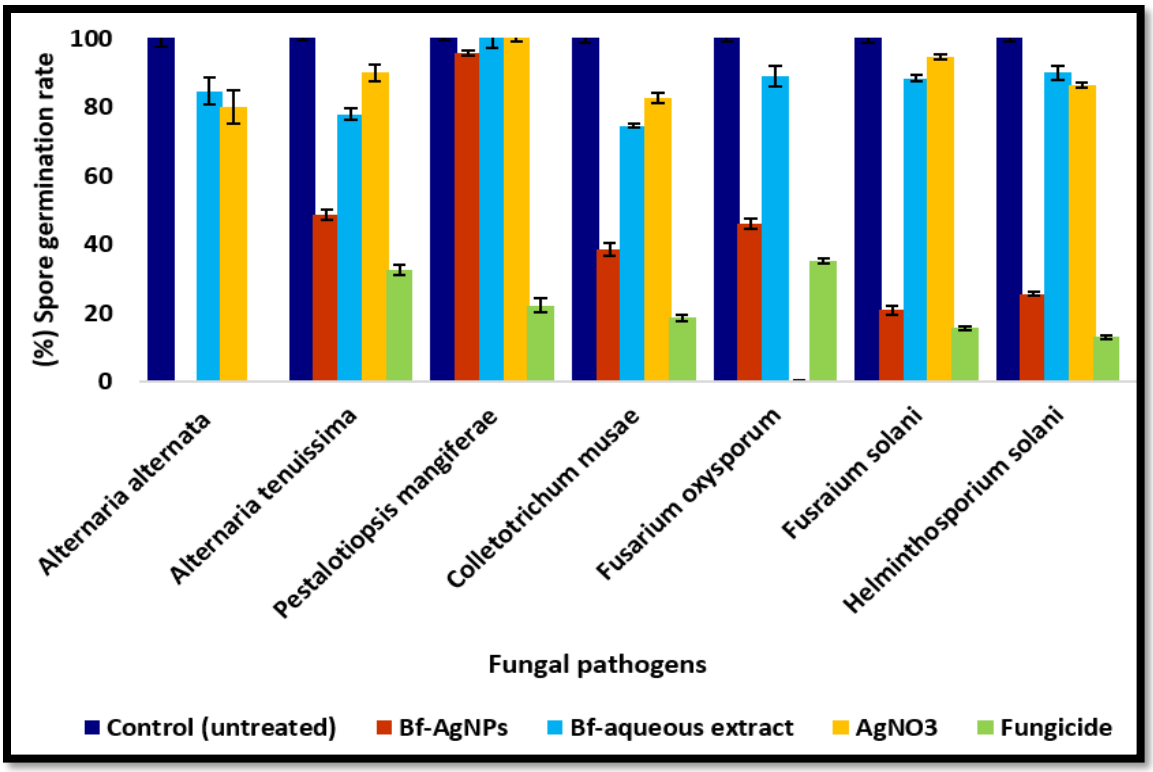
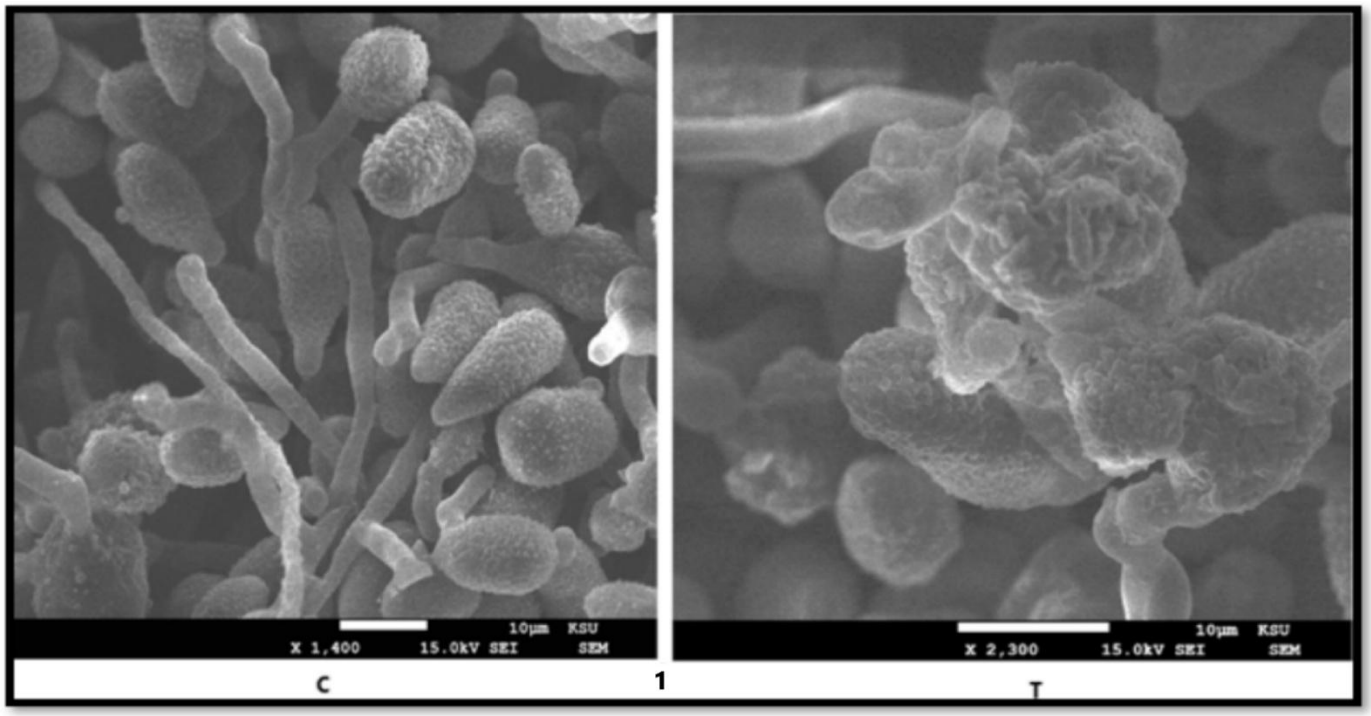


Figure 10. Percentage spore germination of post-harvest fungal pathogens at 50 µg/mL of various treatments (Bf-AgNPs, BF-extract, and tebuconazole). Data represent the mean of three replicates (±SD). Differences among treatments were assessed using one way ANOVA followed by Tukey's HSD test ($p \leq 0.05$).

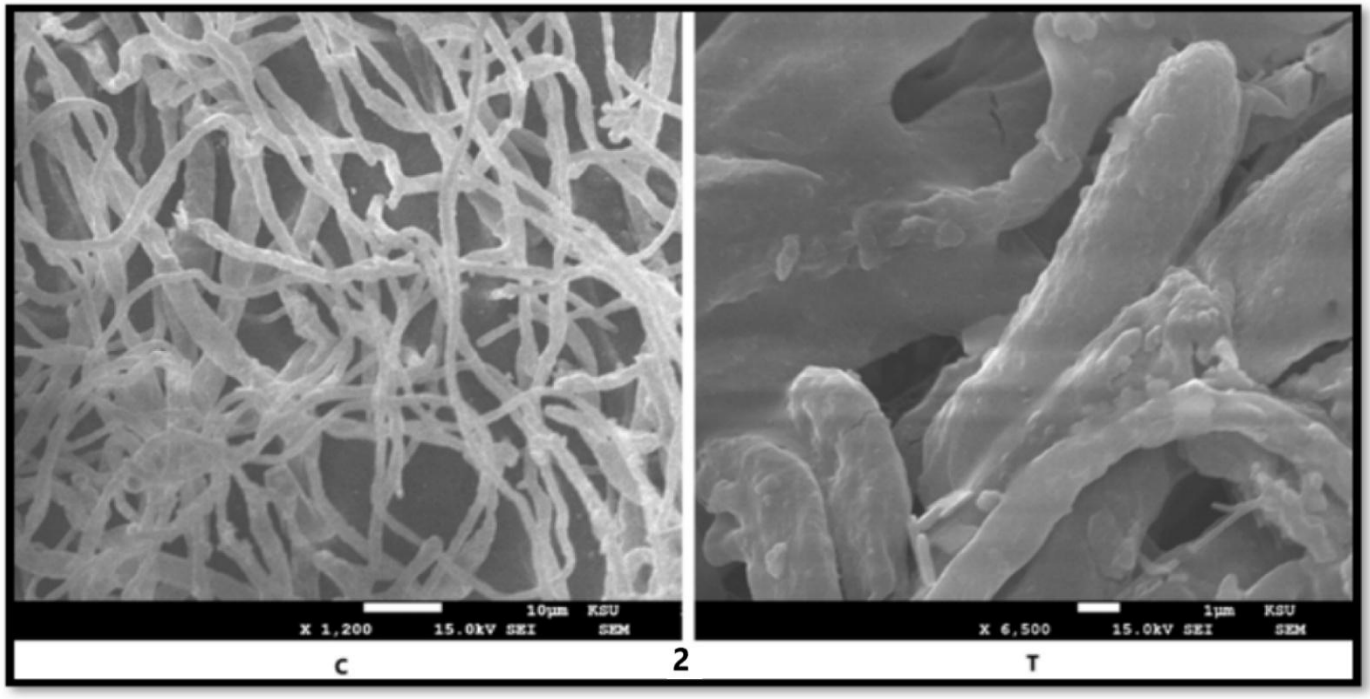
3.5 Scanning electron microscopy

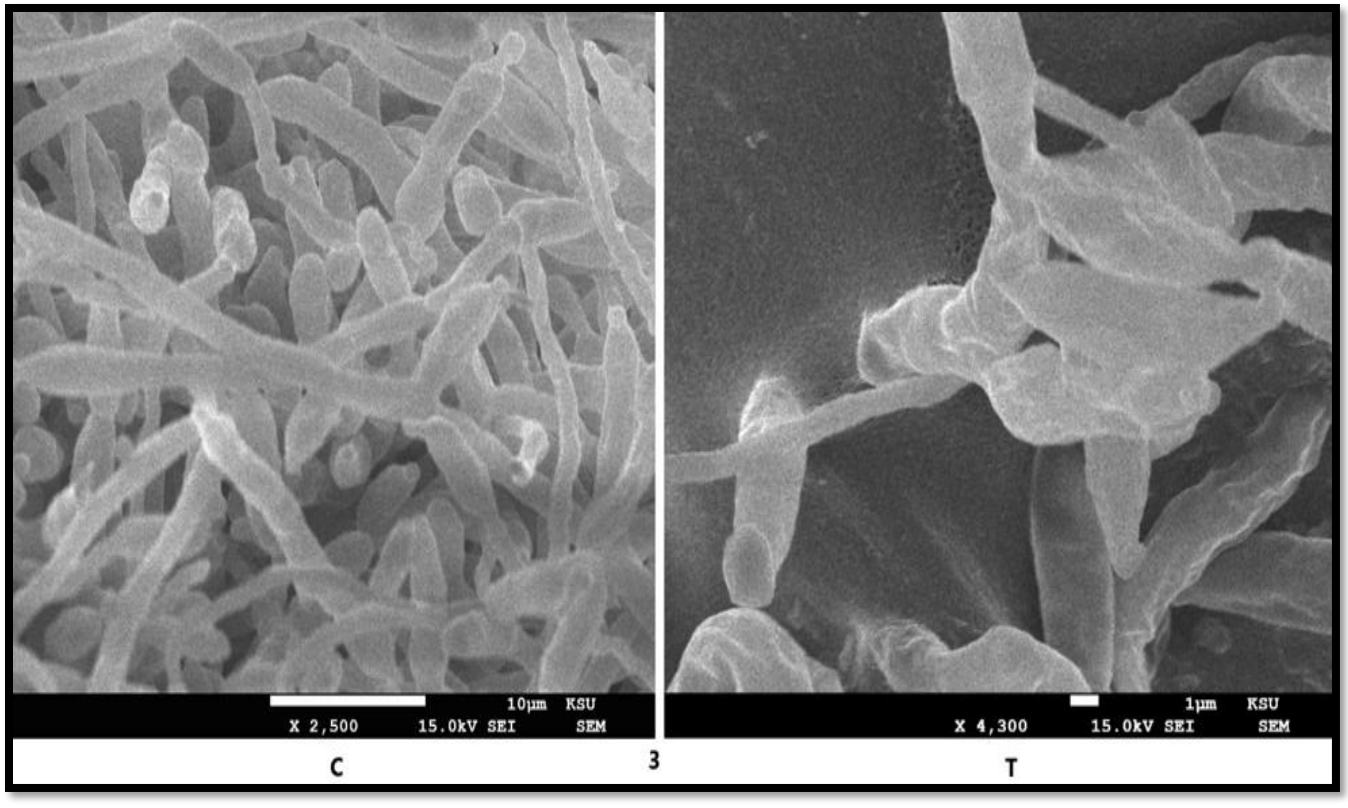
The morphological alterations caused by Bf-AgNPs at their MIC concentrations were selected and subjected to SEM studies. Untreated samples were also selected for comparison. All the fungal test isolates were screened except *Pestalotiopsis mangiferae*, which did not show inhibition in the in vitro assay. All fungal pathogen samples treated with Bf-AgNPs showed clear morphological deformities, but the extent and nature of the damage varied among isolates (Figure 11, T1 to T6). In contrast, the untreated control fungal samples displayed normal structural features, including smooth, intact conidial margins and tubular mycelia with well-defined boundaries (Figure 11, C1 to C6). As shown in Figure 11 (1-T), *A. alternata* mycelium and conidia were markedly distorted with a corrugated surface; *F. solani* exhibited commingled, stout and distorted hyphae, and its conidial structures had lost their original

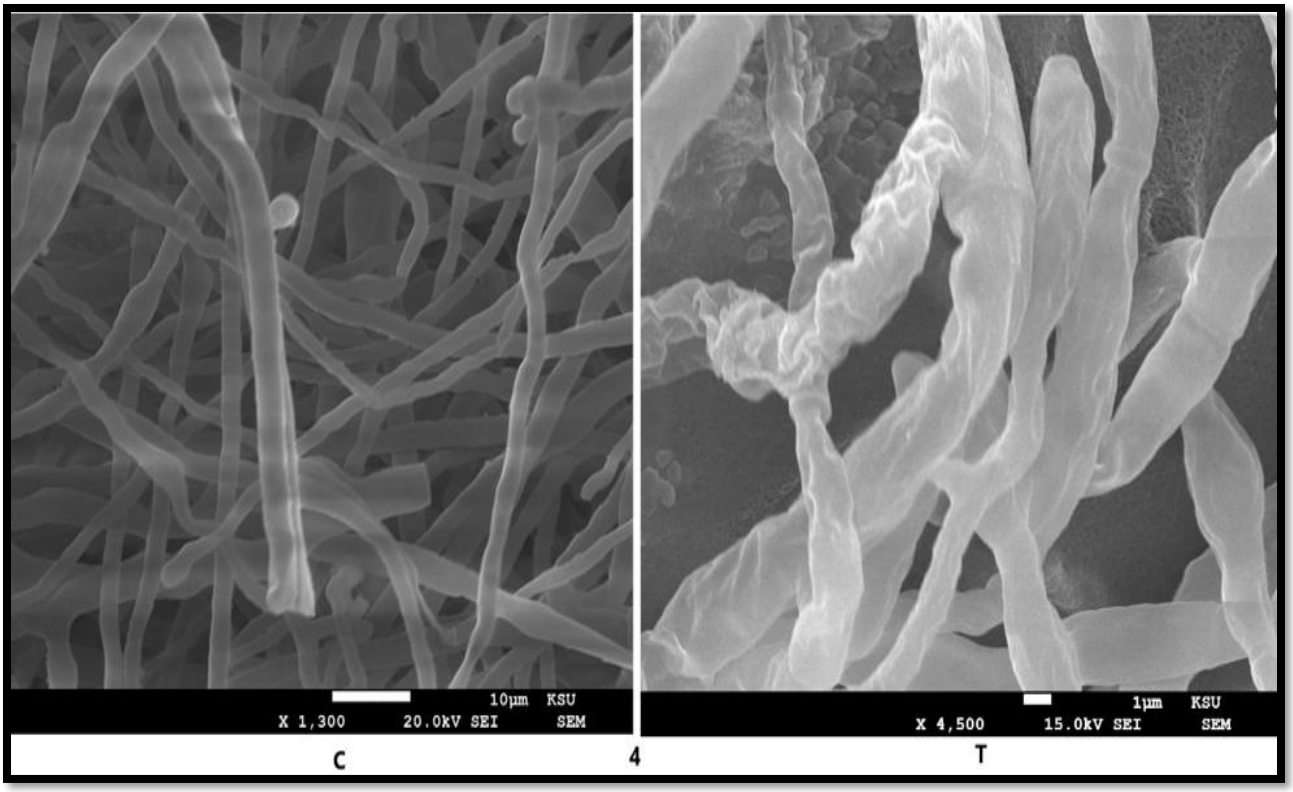
shape (Figure 11 (2-T)). Figure 11 (3-T) shows severely deformed, misshapen conidia and disfigured mycelia of *F. oxysporum*. The *H. solani* isolate showed indented, crooked, and completely contorted mycelial and conidial structures (Figure 11, 4-T). Figure 11 (5,6-T) clearly depicts swollen, stout, and structurally altered mycelium of *C. musae* and *A. tenuissima*, with conidia that appeared leaky and corrugated.



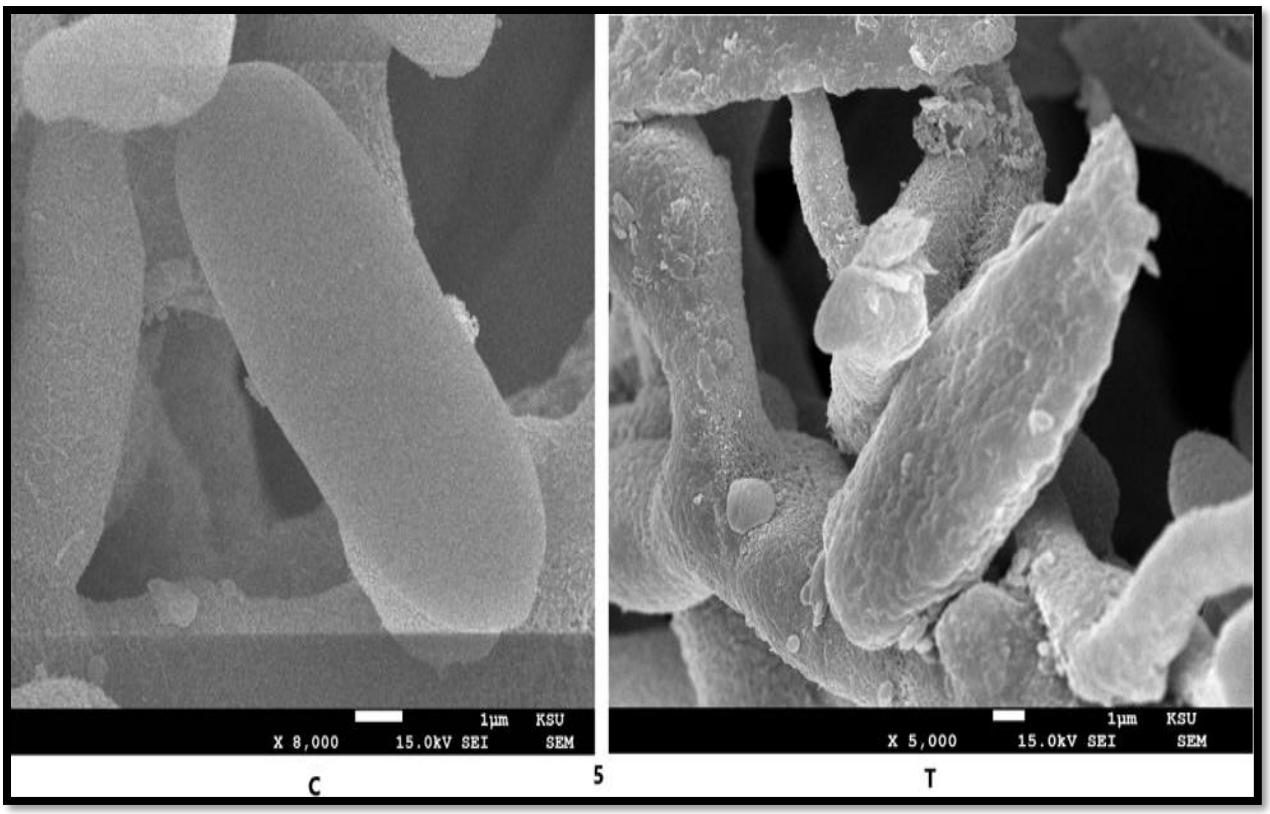
3


10µm KSU
X 1,200 15.0kV SEI SEM
1µm KSU
X 6,500 15.0kV SEI SEM
C
2
T


10µm KSU
X 2,500 15.0kV SEI SEM
1µm KSU
X 4,300 15.0kV SEI SEM
C
3
T


10µm KSU
X 1,300 20.0kV SEI SEM
1µm KSU
X 4,500 15.0kV SEI SEM

C 4 T


1µm KSU
X 8,000 15.0kV SEI SEM
1µm KSU
X 5,000 15.0kV SEI SEM

C 5 T

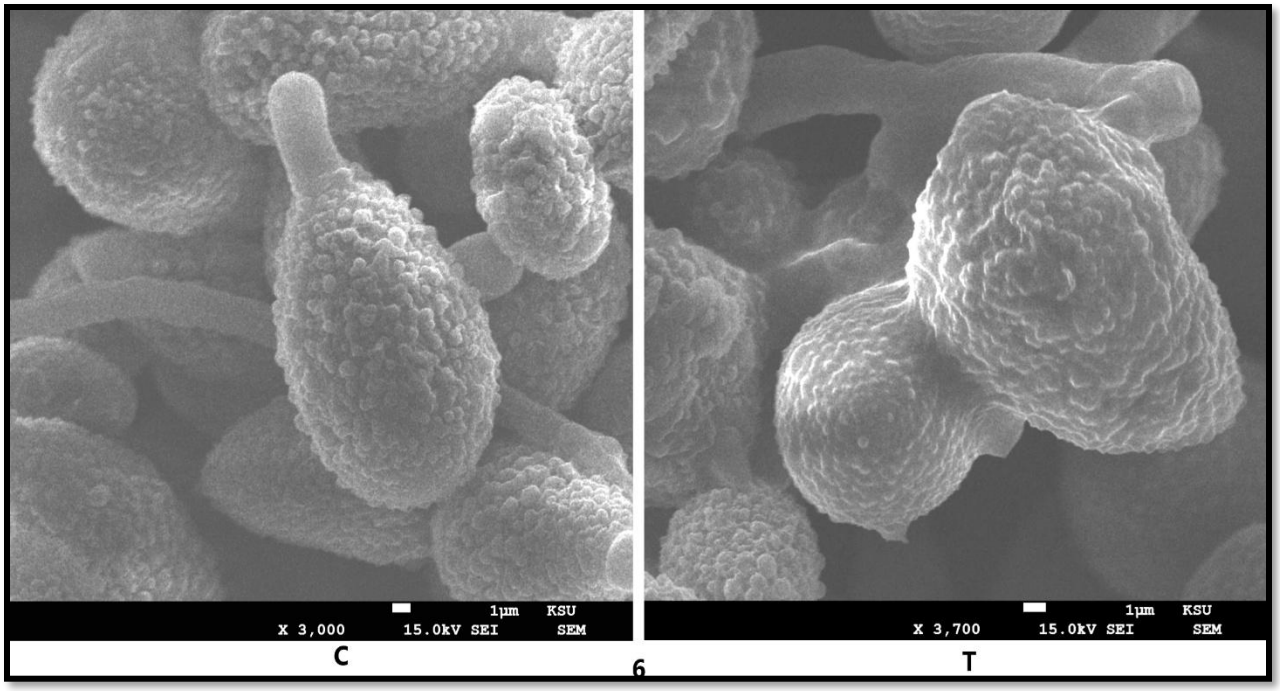


Figure 11. Scanning electron micrographs of Bf-AgNP-treated fungal isolates (C) Control (untreated); (T)-Treated with Bf-AgNPs (*1) Alternaria alternata f. sp. lycopersici (2) Fusarium solani (3) Fusarium oxysporum (4) Helminthosporium solani (5) Colletotrichum musae (6) Alternaria tenuissima*

3.6 MTT assay and cellular morphological changes

The cytotoxic effects of Bf-extract and Bf-AgNPs on HEp-2 and A549 cell lines were assessed using the MTT assay, and the results showed a dose-dependent pattern. (Figure 12A, B). Bf-AgNPs exhibited significant cytotoxic activity against both cell lines (HEp-2 and A549), quite comparable to the robust cytotoxicity of the positive control (doxorubicin). However, the Bf-aqueous extract showed poor cytotoxicity against both cell lines. At 50 µg/mL, the Bf-AgNPs caused a mild reduction in cell viability; however, as the concentration increased, the inhibition also increased. A marked reduction was observed at 100 µg/mL, as the NPs decreased cell viability to approximately 64.45% and 60.35% in HEp-2 and A549, respectively, compared to the control ($P = 0.05$). The IC_{50} values further supported this trend, with AgNPs exhibiting IC_{50} values of 99.2 µg/mL for A549 and 86.6 µg/mL for HEp-2. In contrast, the extract alone showed weaker cytotoxicity, with IC_{50} values of 194.5 ± 3.16 µg/mL for A549 and 188.5 ± 2.26 µg/mL for HEp-2 (Figure 12).

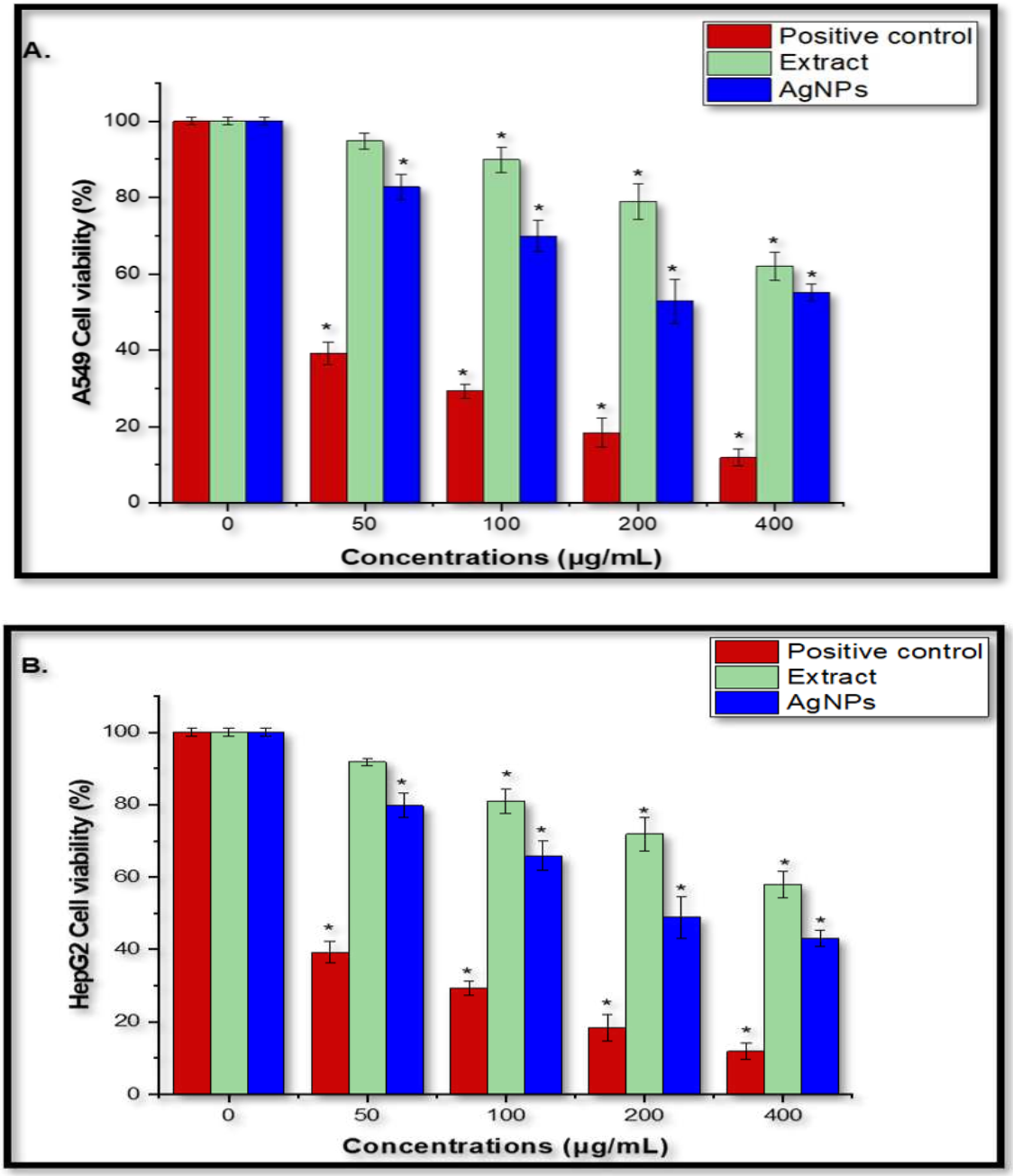


Figure 12. Effect of Bf-extract and Bf-AgNPS on HEp-2 (A) and A549 (B) cell viability after 24 h, as measured by the MTT assay. Cells were treated with the extract and AgNPs (0-400 µg/ml) for 24 h, and viability was quantified using the MTT assay. Data represent the mean ± SD from three independent experiments, with significant differences indicated (* = $p < 0.05$).

3.7. DPPH Radical Scavenging Assay

The radical-scavenging activity of Bf-AgNPs showed notable antioxidant potential (86%) at the highest test concentration (500 µg/mL), indicating a steady increase with concentration (Figure

13). The IC_{50} values were 83.33 µg/mL for the Bf-AgNPs and 59.09 µg/mL for ascorbic acid. The lower IC_{50} value for ascorbic acid indicates a stronger free-radical-scavenging capacity than that of Bf-AgNPs.

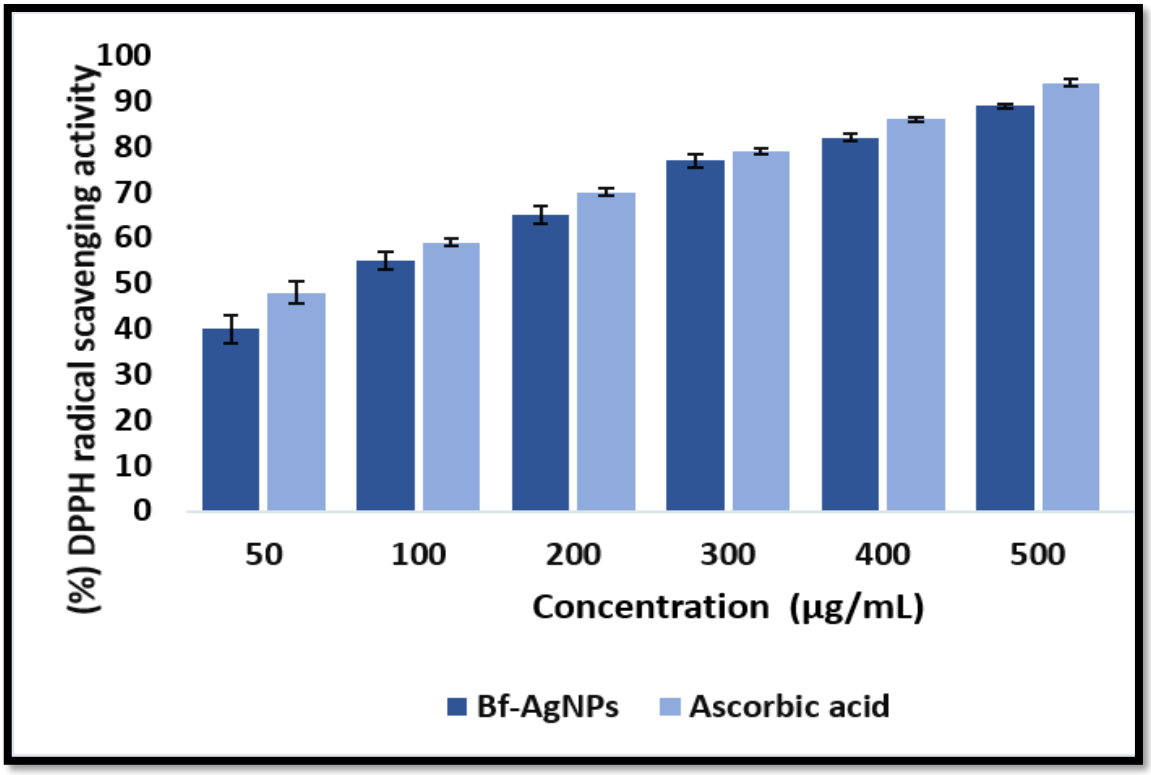


Figure 13. DPPH free radical scavenging activity of Bf-AgNPs

3.8 GC-MS analysis of banana flower extract

GC-MS analysis of the banana flower extract revealed a number of phytochemicals including long chain alcohols, fatty acid esters, nitrogen containing heterocyclics and hydrocarbons (Table 2). A total of 23 compounds were identified by comparison of their mass spectra with the NIST library database. The major compounds were 1,2,5-oxadiazol-3-amine (15.81%), behenic alcohol (12.64%), 1-heneicosanol (12.61%) and 2-amino-4-hydroxy-6,8-dimethyl-7(8H)-pteridinone (8.75%). Other compounds identified were 9-tricosene (Z)-, 10-methylnonadecane, hexadecanoic acid methyl ester and 9,12-octadecadienoic acid methyl ester. The compounds identified in the GC-MS analysis based on both their abundance (area %) and quality were selected for further molecular docking studies to look at their potential interaction with the target protein.

Table 2**. GC-MS phytochemical profile of methanolic extract of banana flower extract**

S.no	Compound	Retention time	Molecular formula	Molecular weight(g/mol)	Area %
1	Cyclotetrasiloxane, octamethyl	14.427	C8H24O4Si4	296.61	0.83

2	Oxalic acid, isobutyl nonyl ester	18.313	C15H28O4	272.38	1.01
3	Hexadecanoic acid, methyl ester	43.226	C17H34O2	270.5	1.96
4	9,12-Octadecadienoic acid (Z,Z)-, methyl ester	47.194	C19H34O2	294.5	0.25
5	Bromoacetic acid, octadecyl ester	51.319	C20H39BrO2	391.4	1.12
6	Tritetracontane	51.799	C43H88	605.2	1.56
7	9-Tricosene, (Z)-	54.543	C23H46	322.6	5.94
8	1,2-Bis(trimethylsilyl)benzene	54.638	C12H22Si2	222.47	0.90
9	10-Methylnonadecane	54.87	C20H42	282.5	4.75
10	1-Heneicosanol	56.991	C21H44O	312.6	12.61
11	Cyclotrisiloxane, hexamethyl-	57.073	C6H18O3Si3	222.46	2.07
12	3-Methoxy-2,4,5-trifluorobenzoic acid, nonadecyl ester	57.237	C27H43F3O3	472.6	1.93
13	Behenic alcohol	59.256	C22H46O	326.6	12.64
14	n-Tetracosanol-1	59.344	C24H50O	354.65	1.41
15	1-Heptacosanol	62.133	C27H56O	396.73	7.81
16	Methyltris(trimethylsiloxy)silane	65.501	C10H30O3Si4	310.68	2.5
17	1H-Indole, 1-methyl-2-phenyl	66.151	C15H13N	207.27	1.00
18	Cyclobarbital	66.246	C12H16N2O3	236.27	7.84
19	2-Amino-4-hydroxy-6,8-dimethyl-7(8H)-pteridinone	67.671	C8H9N5O2	207.19	8.75
20	2-Ethylacridine	68.630	C15H13N	207.27	0.73
21	5-Methyl-2-phenylindolizine	68.656	C15H13N	207.27	0.63
22	Silane, triethyl(2-phenylethoxy)	69.129			5.92
23	1,2,5-Oxadiazol-3-amine, 4-(4-methoxyphenoxy)	69.495	C9H9N3O3	207.19	15.81

3.9 Molecular docking

Table 3 presents the most favourable docking scores for the seven selected compounds and two reference antifungal drugs against sterol 14α-demethylase (CYP51B). For each compound, the pose with the most negative Vina score among the five predicted binding modes was selected, as revealed in Figure 14. Figure 14 shows the selected poses, and Supplementary Table S1 provides the complete docking results and cavity parameters. The best Vina scores for hexadecanoic acid, methyl ester; 9,12-octadecadienoic acid, methyl ester; 1-heneicosanol; behenic alcohol; n-tetracosanol; 1-heptacosanol; and (Z)-9-tricosene were −5.8, −6.3, −5.8, −6.1, −6.1, −6.3, and −6.2 kcal/mol, respectively. Among these compounds, 9,12-octadecadienoic acid, methyl ester and 1-heptacosanol showed the most favourable docking scores, followed by (Z)-9-tricosene. Behenic alcohol and n-tetracosanol shared the same score, as did hexadecanoic acid, methyl ester and 1-heneicosanol. The best Vina scores for tebuconazole and propiconazole were −7.5 and −7.8 kcal/mol, respectively. Under the docking conditions used, both reference drugs had more negative scores than the seven selected compounds.

Table 3. The most favourable CB-Dock scores of selected compounds of banana flower extract and two reference antifungal drugs against sterol 14α-demethylase (CYP51B; PDB ID: 4UYM).

S.No	Compound Name	PubChem CID	Best Vina score (kcal/mol)
1	Hexadecanoic acid, methyl ester	8181	-5.8
2	9,12-octadecadienoic acid methyl esters	5284421	-6.3
3	1-Heneicosanol	85014	-5.8
4	Behenic alcohol (Docosanol)	12620	-6.1
5	n-Tetracosanol	10472	-6.1
6	1-Heptacosanol	74822	-6.3
7	9-Tricosene (Z)	5365075	-6.2
8	Tebuconazole	86102	−7.5
9	Propiconazole	43234	−7.8

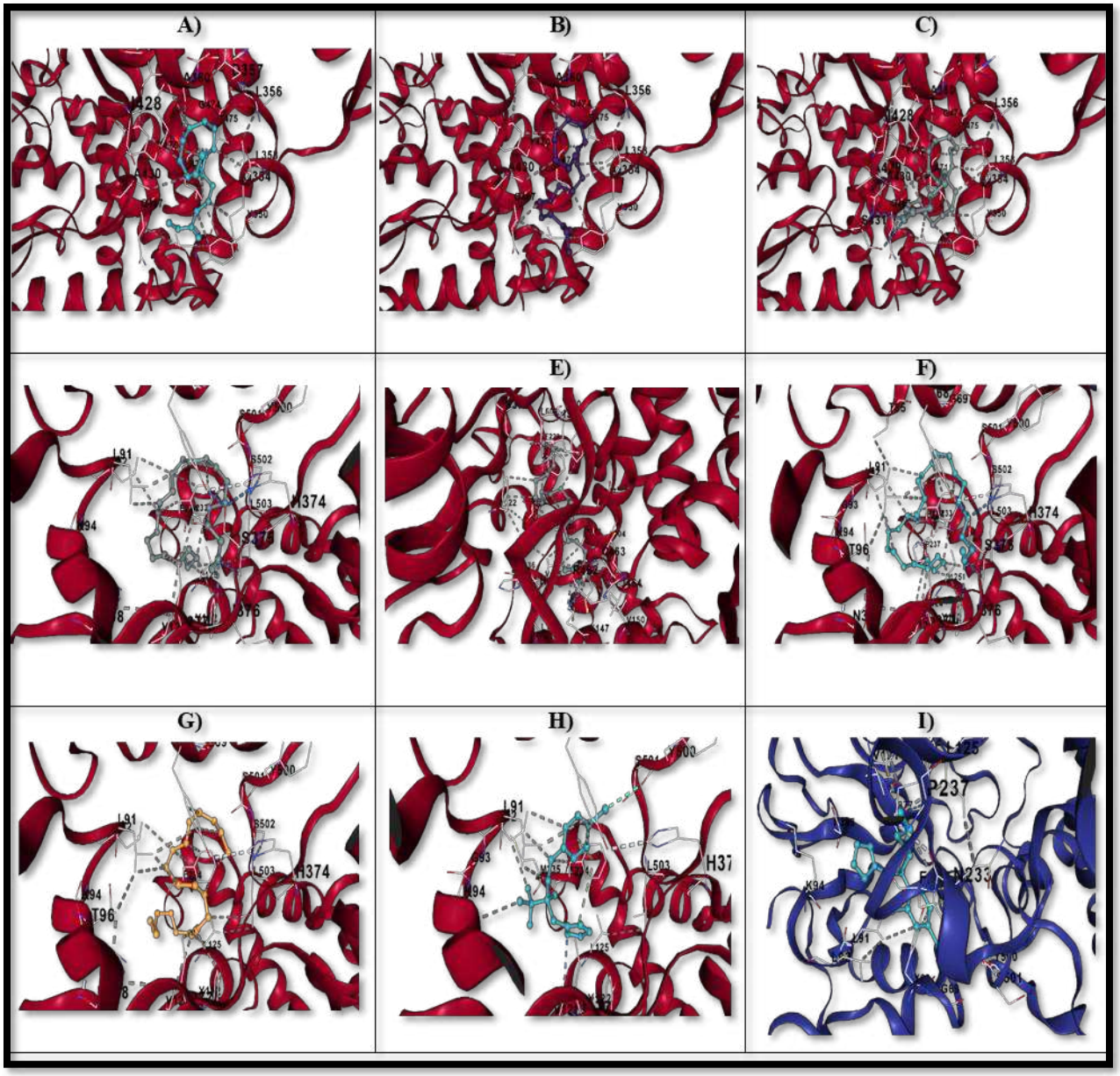


Figure 14. Top-ranked binding poses of selected compounds docked to sterol 14α-demethylase (CYP51B; PDB ID: 4UYM) using CB-Dock. (A) Hexadecanoic acid, methyl ester; (B) 9,12-octadecadienoic acid, methyl ester; (C) 1-heneicosanol; (D) behenic alcohol (docosanol); (E) n-tetracosanol; (F) 1-heptacosanol; and (G) (Z)-9-tricosene (H) Tebuconazole; (I)Propiconazole. The figure shows the pose with the most negative Vina score among the five reported binding modes for the corresponding compound.

4. Discussion

Globally, postharvest losses of fruits and vegetables remain a major concern. These losses reduce quality and shelf life, affecting marketability [23,24]. Fungal pathogens are considered major contributors, as they cause spoilage during growth, harvest, postharvest, storage and

transport [22]. Chemical fungicides are widely employed to control postharvest fungal diseases. Their excessive and often indiscriminate use poses serious concerns as environmental pollutants and affects human and animal health [26]. In addition, the growing population of fungicide-resistant fungal strains has intensified the need for safer, eco-friendly, and sustainable alternatives for postharvest disease management [26]. Green nanotechnology has emerged as a promising solution because of its simplicity, affordability, and reduced ecological footprint. Among various nanomaterials, plant-mediated silver nanoparticles have gained considerable attention for their potent antimicrobial properties and potential application in postharvest disease management. Hence, in this study, we explored the potential of Banana flowers grown in Saudi Arabia for their antifungal properties against some selected postharvest pathogens.

In this study the formation of Bf-AgNPs was evident from the colour change, as the mustard-coloured aqueous extract of banana flowers changed to a brown suspension upon addition of 1 mM AgNO3 solution and subsequent exposure to sunlight at room temperature. The nanosynthesis was carried out using sunlight in accordance with a previously described method [23]. The colour change was rapid under direct sunlight, and the suspension began to turn brown in about 12 minutes; however, it stabilized after 17 minutes with no further change, indicating complete reduction and the formation of Bf-AgNPs (Figure 1). When the colour of the reaction mixture ceased to change, it indicated that the Ag+ ions had been completely reduced and Bf-AgNPs had been formed. This is consistent with previous reports in which nanoparticle formation has been reported in as little as 9 minutes [29] and 3 minutes [43]. Plant extracts are rich in a variety of bioactive phytochemicals (flavonoids, phenols, etc.) that can chelate and reduce metal ions such as silver. As such, nanoparticle formation via plant extracts is typically much faster than in other green synthesis methods such as microbial synthesis [44,45].

The bioactive compounds in banana flowers were found to reduce Ag+ ions ($AgNO_3$) to Ag0 and to aid nanoparticle formation via nucleation, capping, and stabilization. The prominent LSPR band (λmax = 422 nm) confirmed Bf-AgNPs formation and is indicative of the characteristic optical behaviour of metallic silver nanoparticles formed under sunlight-mediated reduction. This is in line with an earlier study on banana flower [46].

The findings of this study show that electromagnetic radiation from sunlight could have enhanced the nanosynthesis process, as described in earlier studies [23,29,47]. According to Khade et al., electromagnetic energy, especially the incident photon energy, drives the reduction of silver ions, promoting rapid nucleation and resulting in colloidally stable NPs [47,48]. The effects of red, green, blue, yellow, and UV light on nanosynthesis and particle size formation showed that blue light produced 59.7 mm NPs, which were much smaller than those produced by the other wavelengths [38-47]. Another study showed that blue light in sunlight is vital in the reduction process (Ag+ to Ag) [48], as the blue light causes tautomerization of flavonoids, which causes the release of hydrogen atoms that could possibly influence the reduction process of Ag+ ions [49]. Hence, it can be inferred from this study that mild thermal heating from sunlight could have slightly raised the reaction temperature, accelerating the reduction of Ag^+ ions, faster nucleation, growth and stabilization of NPs during sunlight assisted Bf-AgNP synthesis

The nanoparticle size was assessed using both transmission electron microscopy (TEM) and dynamic light scattering (DLS). These two techniques produced slightly different sizes

(measurements) because they operate on fundamentally different principles. TEM basically provides the core diameter of the Bf-AgNPs under dry conditions, making it easy to observe surface morphology and physical dimensions [50]. In contrast, DLS measures the hydrodynamic diameter of nanoparticles in suspension, which is influenced by Brownian motion and light-scattering intensity. The difference in nanoparticle sizes observed in TEM and DLS studies arises because DLS measures the metallic core along with adsorbed biomolecules, the surrounding solvation layer, and any surface coating. Hence, the size of NPs in DLS measurements is always larger than in TEM measurements [43,51]. In a previous study, AgNPs synthesized using banana flower extract were spherical, with an average size of 47nm, which closely aligns with our findings [52].

The FTIR spectrum of the banana flower extract showed peaks corresponding to O–H, C–H bending, C=C, N–H, and C=O stretching vibrations, highlighting the rich diversity of bioactive compounds in the Bf-extract. Phenolics, flavonoids, hydroxyl, carbonyl, aromatic compounds, and amines are known to participate in bioreduction and capping, as reported in earlier studies on banana flower extract [52,53,54,55]. The FTIR spectrum of BF-AgNPs showed peaks similar to those in the extract spectrum, retaining many peaks at similar positions; however, some peaks shifted in position and intensity, particularly at 1721 cm^{-1} and 1635 cm^{-1}. These shifts indicate that hydroxyl, carbonyl, and amide groups actively reduced Ag^{+} to Ag^{0} and subsequently adhered to the nanoparticle surface, forming a stabilizing capping layer. Previous studies have documented similar spectral changes [43,50,56]. The disappearance of peaks at 2856 cm^{-1}, 1377 cm^{-1}, and 1108 cm^{-1} in the Bf-AgNP spectrum suggests that the aliphatic C–H, C–H bending, and C–O functional groups were either consumed or became tightly bound during nanoparticle formation, confirming their direct involvement in reduction and capping [56,57,58]. In contrast, the appearance of new peaks at 1255 cm^{-1} and 917 cm^{-1} exclusively in the Bf-AgNP spectrum indicates the formation of fresh biomolecule silver interactions during nanosynthesis. Additionally, the distinct band at 590 cm^{-1} corresponds to Ag–O or metal biomolecule vibrations, confirming successful nanoparticle formation and effective capping [59].

Therefore, the spectral changes indicate that the phytochemicals in banana flower extract acted as both reducing and stabilizing agents during the green synthesis of Bf-AgNPs. These findings are consistent with earlier reports on banana flower extract and other plant-mediated AgNPs, where similar peak shifts, the appearance of new bands, and the disappearance of peaks have been attributed to bioreduction, capping, prevention of agglomeration, and improved nanoparticle stability [51,52,54,60].

The XRD pattern of the Bf-AgNPs clearly confirms successful nanoparticle formation and their crystalline nature. The well-defined Bragg peaks for cubic silver are typically observed at (101), (111), (200), (220), and (311) planes, corresponding to the face centred cubic (fcc) structure of metallic silver, matching the standard JCPDS reference for Ag^{0} (No. 04-0783). The peak intensity at the (111) diffraction plane suggests thermodynamically stable crystal growth. Similarly strong (111) peaks have also been reported for green synthesized AgNPs, including those produced using banana flowers and other plant extracts. [28,43,52,54]. The absence of additional peaks indicates purity, as reported in previous studies [43,50,61].

The EDS spectrum confirmed silver as the major element. The additional peaks for sodium, chlorine, potassium, and calcium originate from phytochemicals present in the banana flower extract that remain associated with the nanoparticle surface during reduction and capping. The carbon peak most likely arose from the carbon coated copper grid used during analysis. A similar elemental profile with a dominant silver peak and minor signals from plant derived elements has been reported for AgNPs synthesized using banana flower and other plant extracts, and our findings align well with these earlier studies [23,52].

The in vitro and spore germination assays clearly demonstrate that Bf-AgNPs possess strong antifungal activity, particularly in their ability to significantly suppress spore germination. In contrast, aqueous banana flower extract and $AgNO_3$ solution alone showed minimal inhibition of mycelial growth and spore germination, indicating enhanced bioactivity through nanoparticle synthesis. Green synthesized silver nanoparticles inhibit fungal growth and spore germination by disrupting cellular stability, altering membrane permeability, and interfering with respiratory processes [50,52,62]. Saha et al. reported that AgNPs synthesized from *Musa paradisiaca* at 40 $\mu g\ mL^{-1}$ effectively suppressed mycelial growth and key infection structures, such as spore germination and appressorium formation, in *Pyricularia oryzae* (*Magnaporthe oryzae*), the causal agent of rice blast disease, as these structures are essential for host penetration and successful disease establishment [52]. Earlier studies have demonstrated significant inhibitory effects of plant-derived AgNPs on mycelial growth in a wide range of phytopathogens, including *Aspergillus niger*, *A. flavus*, *Penicillium* spp., *Cladosporium* spp., *Alternaria* spp., *Fusarium solani*, *F. graminearum*, and several other fungal species [50,63,64]. These findings collectively reinforce the broad-spectrum antifungal potential of green-fabricated silver and other metal nanoparticles.

Although earlier studies have used banana flower extracts to synthesize AgNPs, they have not thoroughly explored flowers grown in Saudi Arabia against fungal plant pathogens used in this study; however, earlier reports show the effect of paradisiaca against several phytopathogenic bacteria and fungal isolates such as *Macrophomina phaseolina*, *Botrytis cinerea*, *Alternaria alternata* and *Pyricularia oryzae* [52,65,66]. Previous studies have shown saponins, steroids, glycosides, flavonoids (quercetin), tannins, triterpenes, and phenols in flowers of *Musa acuminata* and other *Musa species* [3,66]. Besides, a study showed that Cavendish banana flowers possess a high amount of anthocyanin (130.01 mg/100 g), which was dominated by cyanidin, followed by malvidin, pelargonidin, peonidin, delphinidin, and petunidin, all of which are known to contribute to antimicrobial, anticancer and antioxidant properties [66]. The findings of the present study are consistent with previous studies, which attribute the potent antifungal activity to phytochemicals such as phenols, flavonoids, and anthocyanins, as well as to a synergistic effect, further validating our findings [23,50,52,66]. This notable antifungal activity highlights the potential of Bf-AgNPs in postharvest disease management. However, further studies are needed to assess their efficacy and safety under postharvest conditions before practical application.

SEM micrographs of phytopathogens treated with Bf-AgNPs showed extensive morphological alterations and structural deformities. Fungal samples treated with Bf-AgNPs showed severely damaged, swollen hyphae; besides, hyphae were swollen, commingled, and irregularly stout, and the conidia were severely ruptured, coalesced, and completely deformed.

Such morphological deformities highlight the potent antifungal activity of Bf-AgNPs and suggest that their inhibitory action probably involves multiple cellular targets. Although the precise mechanism by which silver nanoparticles act on microbial cells is not yet fully understood, substantial evidence, particularly from earlier studies on green-synthesized AgNPs, indicates that nanoparticles employ multiple, simultaneous pathways to exert antifungal activity [67,68,69]. The most widely accepted view is that AgNPs initially interact with the fungal cell surface, releasing Ag^{+} ions that readily bind to structural polymers such as chitin and β-glucans. This interaction weakens the cell wall and destabilizes the plasma membrane by disturbing lipid and protein organization and impairing normal osmotic regulation. Consequently, the cell surface becomes visibly deformed, showing pitting, erosion, and pore formation reflecting the severe structural stress imposed by AgNP exposure [70,71,72].

Another proposed mechanism suggests that ions released from silver and copper nanoparticles can interact directly with fungal DNA, inducing genotoxic effects. These ions may intercalate between nucleic acid bases, deform DNA structure, trigger mutations, and cause chromosomal aberrations along with other nuclear deformities [73,74,75]. It has also been suggested that the influx of AgNPs into the cytoplasm due to increased permeability disrupts organelles, molecules and all vital metabolic functions of the fungal cells, including nuclear fragmentation, membrane depolarisation, and an increase in ROS production, which leads to apoptosis and cell death [70,76,77]. Additionally, high levels of ROS affect lipid peroxidation, cause DNA damage, and protein denaturation [70,78] which can also disrupt the cell wall and membrane, leading to pore formation, cell leakage and cell death [70,79]. Consistent with our SEM findings, previous reports have described morphological deformities in various fungal species, including *Alternaria, Fusarium, Aspergillus,* and *Colletotrichum*, when treated with green silver nanoparticles [50,80]. In the present study, the varying responses of the tested pathogens to Bn-AgNPs may be due to species-specific differences in their cell membrane compositions and cell wall structures, as well as differences in the defense mechanisms and response to nanoparticle uptake.

The MTT assay clearly demonstrated that Bf-AgNPs induce a concentration-dependent cytotoxic response in both A549 and HEp-2 cell lines. To date, no studies have specifically reported the cytotoxicity of banana flower mediated silver nanoparticles against Hep-2 or A549 cells. Earlier studies on the flowers and bracts of *Musa paradisiaca*, *Musa acuminata*, and other *Musa* species provide strong supportive evidence that extracts and bioactive fractions from flowers and bracts possess notable anticancer potential [15,81,82]. Putri et al., reported that the ethyl acetate fraction of banana bracts markedly suppresses HeLa cell proliferation, downregulates EGFR and Ki-67 expression, and activates apoptotic pathways [81]. Our findings are consistent with the above citied studies further validating the findings of this study.

Banana flower extract has also shown dose-dependent cytotoxicity against SiHa cells (1–200 µg/mL), with anthocyanins identified as the major contributors that can induce apoptosis [83]. Similarly, *Musa acuminata* flower extracts inhibited HeLa cell proliferation [82], and the anthocyanin fraction of Nendran banana bracts exhibited cytotoxicity toward HeLa and HT-29 cells [16]. These findings collectively suggest that the phytochemical richness, such as anthocyanins and flavonoids of banana inflorescence function as natural capping biomolecules during nanoparticle synthesis, and contribute towards their role in cytotoxic and antiproliferative activity [4,82,83,84].

Further supporting this, Timsina and Nadumane (2014) demonstrated that the phenolic fraction of *Musa paradisiaca* flower extract exhibited potent antiproliferative activity against HeLa and CHO cells, with IC_{50} values below 10 µg/mL. Comparable cytotoxic responses have also been reported for green synthesized AgNPs, which inhibited A549 and HeLa cell proliferation at 5 and 2 µg/mL, respectively [85]. Green AgNPs induce marked morphological changes in cancer cells, including shrinkage, reduced cell density, and loss of adhesion, as documented in HeLa cells [86], which aligns with the findings of this study. Their cytotoxic action largely stems from excessive generation of reactive oxygen species (ROS), which activate mitochondrial dependent apoptotic pathways. Elevated ROS levels intensify oxidative damage, trigger genotoxic stress, and upregulate apoptosis-related genes [87,88,89].

The DPPH assay showed potent antioxidant activity of Bf-AgNPs in a dose-dependent manner, with an IC_{50} of 83 µg/mL. GC-MS and FTIR analyses of Banana flower extract revealed several phytochemicals. Bioactive compounds such as phenols, anthocyanins, triterpenes and flavonoids have shown free radical scavenging properties in previous studies, as they are strong ROS (reactive oxygen species) scavengers that disrupt free radical chains, chelate metal ions and inhibit enzyme activity [90;17,45,50]. Consistent with this study, previous findings have shown antioxidant activity of banana flower mediated silver nanoparticles and extracts [65,17].

Molecular docking analysis showed that the seven major compounds identified in banana flower extract exhibited notable binding affinities towards sterol 14α-demethylase (CYP51B), with binding energies between −5.8 and −6.3 kcal/mol. Among all the phytochemicals, 9,12-octadecadienoic acid, methyl ester and 1-heptacosanol showed the strongest binding affinities (−6.3 kcal/mol), followed by(Z)-9-tricosene (−6.2 kcal/mol). The docking score provides preliminary computational insight into potential interactions between the target fungal protein (CYP51) and the selected phytochemicals (ligands). As CYP51 plays an important role in ergosterol synthesis, these interactions could contribute to fungal growth inhibition by affecting cell membrane integrity. Nevertheless, the docking results are only predictive evidence; further experimental studies are required to confirm CYP51's involvement in the antifungal mechanism of action. Similarly, previous studies have reported that the antifungal activity of phytochemicals rich in fatty acids and related lipophilic metabolites occurs through disruption of sterol biosynthesis and interactions with membrane-associated targets [91,92], consistent with this study.

Although the predicted binding energies indicate moderate rather than exceptionally strong interactions, the combined effects of multiple phytoconstituents and the intrinsic antimicrobial properties of silver nanoparticles may have contributed to the significant antifungal efficacy observed in this study.

5. Limitations of the study

Although the present study shows promising antifungal activity against postharvest pathogens, the effectiveness of these Bf-AgNPs under postharvest conditions needs to be confirmed through in vivo experiments. Additionally, further studies are needed to confirm the stability, efficacy, biocompatibility, and safety of the synthesized AgNPs for plant tissue and human health. The cytotoxicity assays were not performed on normal cells and were limited to only cancer cell lines; hence, selective biosafety and toxicity could not be assessed. The GC-MS findings were based

solely on NIST library matches, and the identified phytochemicals were neither isolated nor experimentally confirmed. Furthermore, the molecular docking provided valuable insight by offering predictive evidence of ligand-protein interactions, but it requires further experimental validation.The cytotoxicity assays were limited to cancer cell lines, and no normal mammalian cells were included. Therefore, selective toxicity and biosafety could not be assessed

6. Conclusions

This study focused on an eco-friendly plant-based route to synthesize AgNPs from banana flowers grown in Saudi Arabia. The synthesized Bf-AgNPs were characterized and showed an surface plasmon resonance absorption band at 422 nm; the average size of NPs was 18.96 nm, and XRD confirmed their face-centred crystalline structure. FTIR spectra showed functional groups associated with key phytochemicals that may have aided bioreduction and acted as capping ligands. The findings show significant antifungal, cytotoxic, and antioxidant properties of banana flowers. However, further research is needed to evaluate their safety, efficacy, practical applicability, and environmental impact before they are considered an alternative to conventional synthetic fungicides. Furthermore, molecular docking analysis showed that the seven major compounds identified in banana flower extract by GC-MS exhibited binding affinities for sterol 14α-demethylase (CYP51B), with binding energies between −5.8 and −6.3 kcal/mol. However, molecular docking provides only a predictive assessment of ligand-protein interactions and does not establish CYP51B inhibition or direct involvement in the antifungal mechanism. Therefore, further investigation using molecular dynamics simulations, enzyme inhibition studies, and gene expression analyses would help confirm CYP51B involvement in the antifungal mechanism of action and further validate the biological significance of the predicted interactions.

Data availability: The data used in this study are available from the corresponding author upon request.

References

1. Senevirathna, N.; Karim, A. Banana inflorescence as a new source of bioactive and pharmacological ingredients for food industry. Food Chemistry Advances 2024, 5, 100814.

2.FAO (2025). Banana Markets and Trade. Food and Agriculture Organization of the United Nations. https://www.fao.org/markets-and-trade/commodities-overview/bananas-tropical-fruits/bananas/en

3. Wahab, N.B.A.; Ismail, S.N.; Abidin, M. Physicochemical and sensory characteristics of banana blossom nuggets. International journal of research and innovation management 2020, 6, 56–66.

4. Rodrigues, A.S.; Kubota, E.H.; da Silva, C.G.; dos Santos Alves, J.; Hautrive, T.P.; Rodrigues, G.S.; Campagnol, P.C.B. Banana inflorescences: A cheap raw material with great potential to be used as a natural antioxidant in meat products. Meat science 2020, 161, 107991.

5. Zou, F.; Tan, C.; Zhang, B.; Wu, W.; Shang, N. The valorization of banana by-products: Nutritional composition, bioactivities, applications, and future development. Foods 2022, 11, 3170.

6. Safhi, F.A.; Alshamrani, S.M.; Alshaya, D.S.; Hussein, M.A.; Abd El-Moneim, D. Genetic diversity analysis of banana cultivars (Musa sp.) in Saudi Arabia based on AFLP marker. Current Issues in Molecular Biology 2023, 45, 1810-1819.

7. Krishnan, A.; Sinija, V. Proximate composition and antioxidant activity of banana blossom of two cultivars in India. International journal of Agriculture and food science technology 2016, 7, 13–22.

8. Chowdary, M.Y.; Rana, S.S.; Ghosh, P. Banana inflorescence and their potential health benefits as future food. Quality Assurance and Safety of Crops & Foods 2022, 14, 131–136.

9. Panyayong, C.; Srikaeo, K. Effects of hydrocolloids on the qualities of pureed banana inflorescences prepared for individuals with dysphagia. Food Hydrocolloids for Health 2023, 3, 100129.

10. Lau, B.F.; Kong, K.W.; Leong, K.H.; Sun, J.; He, X.; Wang, Z.; Mustafa, M.R.; Ling, T.C.; Ismail, A. Banana inflorescence: Its bio-prospects as an ingredient for functional foods. Trends in Food Science & Technology 2020, 97, 14–28.

11. Rosa, R.H.; Ribeiro Fernandes, M.; Silva de Pádua Melo, E.; Granja Arakaki, D.; Vieira de Lima, N.; Santos Leite, L.C.; Espindola, P.R.; Domingos de Souza, I.; Aragão do Nascimento, V.; Saldanha Tschinkel, P.F. Determination of Macro-and Microelements in the Inflorescences of Banana Tree Using ICP OES: Evaluation of the Daily Recommendations of Intake for Humans. The Scientific World Journal 2020, 2020, 8383612.

12. Ramírez-Bolaños, S.; Pérez-Jiménez, J.; Díaz, S.; Robaina, L. A potential of banana flower and pseudo-stem as novel ingredients rich in phenolic compounds. 2021.

13. Sumathy, V.; Lachumy, S.J.; Zakaria, Z.; Sasidharan, S. In vitro bioactivity and phytochemical screening of Musa acuminata flower. Pharmacologyonline 2011, 2, 27.

14. Amornlerdpison, D.; Choommongkol, V.; Narkprasom, K.; Yimyam, S. Bioactive compounds and antioxidant properties of banana inflorescence in a beverage for maternal breastfeeding. Applied Sciences 2020, 11, 343.

15. Nadumane, V.K.; Timsina, B. Anti-cancer potential of banana flower extract: An in vitro study. Bangladesh Journal of Pharmacology 2014, 9, 628–635.

16. Suman, R.; Kalaimathi, K.; Palanichamy, S.; Sowmiya, R.; Vaganan, M.; Ravi, I.; Uma, S. Anti-cancerous activities of anthocyanins of banana cv. Nendran (Musa sp.) flower bracts against human colon and cervical cancer cell lines. Int. J. Curr. Microbiol. App. Sci 2018, 7, 2786–2793.

17. Suchitra, M.; Bhuvaneswari, S.; Parthasarathy, S. Comparative analysis of phytochemical, antioxidant, antibacterial and anticancer activity of Musa acuminata flower florets and its innermost part kuruthu. 2026.

18.Vilhena, R.; Figueiredo, I.; Baviera, A.; Silva, D.; Marson, B.; Oliveira, J.; Peccinini, R.; Borges, I.; Pontarolo, R. Antidiabetic activity of Musa x paradisiaca extracts in streptozotocin-induced diabetic rats and chemical characterization by HPLC-DAD-MS. Journal of ethnopharmacology 2020, 254, 112666.

19. Gayathry, K.; John, J.A. Phenolic profile, antioxidant, and hypoglycaemic potential of pseudostem and inflorescence extracts of three banana cultivars. Biomass Conversion and Biorefinery 2025, 15, 2387–2395.

20. Peja Jr, R.; Dimayacyac, D.A.; Barcelo, J.; De Torres, R.; Mandap, J.A.; Amas, J.; Duay, S.S.; Zakaria, L.; Cumagun, C.J.; Romanazzi, G. Fungi in the Postharvest of Agricultural Commodities. In Mycology in a Changing Planet: Applications and Perspectives from Southeast Asia; Springer: 2025; pp. 245–300.

21. Karoney, E.M.; Molelekoa, T.; Bill, M.; Siyoum, N.; Korsten, L. Global research network analysis of fresh produce postharvest technology: Innovative trends for loss reduction. Postharvest Biology and Technology 2024, 208, 112642.

22. Prusky, D.B.; Chen, T.; Chen, Y.; Tian, S.; Li, B. Quiescence of postharvest pathogens: a fungal inhibition process or an immune response of the unripe host fruit? New Phytologist 2026, 250, 812–821.

23. Rizwana, H.; Bokahri, N.A.; S. Alkhattaf, F.; Albasher, G.; A. Aldehaish, H. Antifungal, antibacterial, and cytotoxic activities of silver nanoparticles synthesized from aqueous extracts of mace-arils of Myristica fragrans. Molecules 2021, 26, 7709.
24. Ambuko, J.L.; Masakhwe, S.M.; Amwoka, E.; Mujuka, E.; Fabi, C. Food loss and waste data gaps in fruit and vegetable value chains: A review of the literature. Frontiers in Horticulture 2025, 4, 1529040.

25.FAO of United Nations – 2026.https://www.fao.org/sustainable-development-goals-data-portal/data/indicators/1231-global-food-losses/en.

26. Feng, Y.; Shi, J.; Liu, J.; Yuan, Z.; Gao, S. Advancing food safety surveillance: rapid and sensitive biosensing technologies for foodborne pathogenic bacteria. Foods 2025, 14, 2654.

27. Rizwana, H.; Alwhibi, M.S. Biosynthesis of silver nanoparticles using leaves of Mentha pulegium, their characterization, and antifungal properties. Green Processing and Synthesis 2021, 10, 824–834.

28. Kumar, M.; Saini, R.V.; Gupta, M.; Singh, R. Green synthesis of silver nanoparticle (Cha-AgNPs) using Chenopodium album extract and evaluation of their antifungal potential against pathogenic fungi. Biomass Conversion and Biorefinery 2025, 15, 8955–8966.

29. Rizwana, H.; Alwhibi, M.S.; Al-Judaie, R.A.; Aldehaish, H.A.; Alsaggabi, N.S. Sunlight-mediated green synthesis of silver nanoparticles using the berries of Ribes rubrum (red currants): characterisation and evaluation of their antifungal and antibacterial activities. Molecules 2022, 27, 2186.

30. Taher, M.A.; Khojah, E.; Darwish, M.S.; Elsherbiny, E.A.; Elawady, A.A.; Dawood, D.H. Biosynthesis of silver nanoparticles by polysaccharide of Leucaena leucocephala seeds and their anticancer, antifungal properties and as preservative of composite milk sample. Journal of Nanomaterials 2022, 2022, 7490221.

31. Rizwana, H.; Bokahri, N.A.; Alfarhan, A.; Aldehaish, H.A.; Alsaggabi, N.S. Biosynthesis and characterization of silver nanoparticles prepared using seeds of Sisymbrium irio and evaluation of their antifungal and cytotoxic activities. Green Processing and synthesis 2022, 11, 478–491.

32. Kah, G.; Adelusi, O.A.; Gbashi, S.; Awafong, P.M.; Njobeh, P.B. Antifungal and antimycotoxin activity of plant-synthesized silver nanoparticles (AgNPs): A novel approach to combat food contamination. Food Microbiology 2025, 104979.

33.Yang, Q.; Guo, J.; Long, X.; Pan, C.; Liu, G.; Peng, J. Green synthesis of silver nanoparticles using Jasminum nudiflorum flower extract and their antifungal and antioxidant activity. Nanomaterials 2023, 13, 2558.

34. Rizwana, H.; Alzahrani, T.; Alwahibi, M.S.; Aljowaie, R.M.; Aldehaish, H.A.; Alsaggabi, N.S.; Ramadan, R. Phytofabrication of silver nanoparticles and their potent antifungal activity against phytopathogenic fungi. Processes 2022, 10, 2558.

35. Xing, K.; Liu, Y.; Shen, X.; Zhu, X.; Li, X.; Miao, X.; Feng, Z.; Peng, X.; Qin, S. Effect of O-chitosan nanoparticles on the development and membrane permeability of Verticillium dahliae. Carbohydrate polymers 2017, 165, 334–343.

36. Ibrahim, E.; Luo, J.; Ahmed, T.; Wu, W.; Yan, C.; Li, B. Biosynthesis of silver nanoparticles using onion endophytic bacterium and its antifungal activity against rice pathogen Magnaporthe oryzae. Journal of Fungi 2020, 6, 294.

37. Rizwana, H. Postharvest control of anthracnose lesions and its causative agent, Colletotrichum musae by some oils. Cellular and Molecular Biology 2018, 64, 52–58.

38. Kis, B.; Pavel, I.Z.; Avram, S.; Moaca, E.A.; Herrero San Juan, M.; Schwiebs, A.; Radeke, H.H.; Muntean, D.; Diaconeasa, Z.; Minda, D. Antimicrobial activity, in vitro anticancer effect (MCF-7 breast cancer cell line), antiangiogenic and immunomodulatory potentials of Populus nigra L. buds extract. BMC Complementary Medicine and Therapies 2022, 22, 74.

39. Aziz, I.M.; Alshalan, R.M.; Rizwana, H.; Alkhelaiwi, F.; Almuqrin, A.M.; Aljowaie, R.M.; Alkubaisi, N.A. Chemical composition, antioxidant, anticancer, and antibacterial activities of roots and seeds of Ammi visnaga L. methanol extract. Pharmaceuticals 2024, 17, 121.

40. Effiong, M.E.; Umeokwochi, C.P.; Afolabi, I.S.; Chinedu, S.N. Comparative antioxidant activity and phytochemical content of five extracts of Pleurotus ostreatus (oyster mushroom).

41. Liu, Y.; Grimm, M.; Dai, W.-t.; Hou, M.-c.; Xiao, Z.-X.; Cao, Y. CB-Dock: a web server for cavity detection-guided protein–ligand blind docking. Acta Pharmacologica Sinica 2020, 41, 138-144.

42. Cao, Y.; Li, L. Improved protein–ligand binding affinity prediction by using a curvature-dependent surface-area model. Bioinformatics 2014, 30, 1674-1680.

43. Tooba; Assad, N.; Laila, M.B.; Iqbal, R.M.F.; Manahil, L.; Iqbal, J.; Naeem-ul-Hassan, M.; Khuram, A.; Assad, Y.; Khan, M.N. Green synthesis of silver nanoparticles using Solanum lycopersicum leaves extract for highly selective detection of mercury ions and photocatalytic degradation of methylene blue. Discover nano 2026, 21, 14.

44. Adeyemi, J.O.; Oriola, A.O.; Onwudiwe, D.C.; Oyedeji, A.O. Plant extracts mediated metal-based nanoparticles: synthesis and biological applications. Biomolecules 2022, 12, 627.

45. Malik, A.; Liaquat, F.; Azam, M.; Rehman, A.; Qunlu, L.; Shah, I.H.; Qin, J.; Zhang, Y. Multifunctional Nanoparticles for Integrated Management of Plant Fungal Pathogens: From Synthesis to Field Applications. Forest Science and Technology 2026, 1–29.

46. Jegatheesan, G.; Bagyalakshmi, B.; Karthick, K.; Veera Gajendra Babu, M. Green Synthesized Silver Nanoparticles Using Banana Flower Extract—Structural, Optical and Antibacterial Study. In Proceedings of the National Symposium on Recent Advances in Electronic, Optical and Magnetic Materials, 2025; pp. 573–583.

47. Khade, B.S.; Gawali, P.; Ali, M.; Waghmare, M.N.; Dongre, P. Influence of photon and electrical energy in the nucleation of silver nanoparticles synthesis. Journal of Cluster Science 2023, 34, 189–197.

48. Mathew, S.; Prakash, A.; Radhakrishnan, E. Sunlight mediated rapid synthesis of small size range silver nanoparticles using Zingiber officinale rhizome extract and its antibacterial activity analysis. Inorganic and Nano-Metal Chemistry 2018, 48, 139–145.

49. Nguyen, V.T. Sunlight-Driven Synthesis of Silver Nanoparticles Using Pomelo Peel Extract and Antibacterial Testing. Journal of Chemistry 2020, 2020, 6407081.

50. Rizwana, H.; Khan, M.; Aldehaish, H.A.; Adil, S.F.; Shaik, M.R.; Assal, M.E.; Hatshan, M.R.; Siddiqui, M.R.H. Green biosynthesis of silver nanoparticles using *Vaccinium oxycoccos* (Cranberry) extract and evaluation of their biomedical potential. Crystals 2023, 13, 294.

51. Mirzaei, G.H.; Gheybi, F.; Sabouri, Z.; Darroudi, M. Green synthesis of silver nanoparticles using Solanum melongena peel and *Abelmoschus esculentus* extracts: a dual study on antibacterial efficacy and photocatalytic activity. Scientific reports 2026.

52. Saha, C.; Pandit, S.; Hossain, M.M.; Haque, M.M.; Jannat, R.; Rubayet, M.T.; Masum, M.M.I. Eco-friendly biosynthesis of silver nanoparticles from banana flower extract for protective role against the rice blast pathogen *Pyricularia oryzae*. Materials Research Express 2025, 12, 095003.

53. Banu, K.B.; Mary, I.A. Green synthesis and surface functionalization of silver nanoparticles using *Phyllanthus emblica* fruit extract. Discover Chemistry 2026, 3, 489.

54. Weiming, G.; Quanfeng, H.; Jianxia, S.; Dan, L.; Xuejuan, D. Green synthesis of silver nanoparticles using banana flower extract, and their antibacterial activity. International Food Research Journal 2023, 30, 613.

55. Ausha, S.; Praveen, C.; Praveena, M.; Jayanthi, M.; Sivakumar, V. Study of antimicrobial activity in silver nanoparticles from Musa paradisiaca. Journal of Pharmacognosy and Phytochemistry 2021, 10, 94–102.

56. Iskakova, Z.; Kozhantayeva, A.; Temirbekova, A.; Mukhtubayeva, S.; Bissenova, G.; Tekebayeva, Z.; Almagambetov, K.; Tashenov, Y.; Sarmurzina, Z. Green synthesis of silver nanoparticles using *Circaea lutetiana* ethanolic extract: Phytochemical profiling, characterization, and antimicrobial evaluation. International Journal of Molecular Sciences 2025, 26, 5505.

57. Pasupuleti, V.R.; Prasad, T.; Shiekh, R.A.; Balam, S.K.; Narasimhulu, G.; Reddy, C.S.; Rahman, I.A.; Gan, S.H. RETRACTED: Biogenic silver nanoparticles using *Rhinacanthus nasutus* leaf extract: synthesis, spectral analysis, and antimicrobial studies. International journal of nanomedicine 2013, 3355–3364.

58. Bantho, S.; Naidoo, Y.; Dewir, Y.H.; Singh, M.; Lin, J.; Bantho, A. Synthesis, Characteristation and Biological Activity of Silver Nanoparticles Generated Using the Leaf and Stembark Extract of *Combretum erythrophyllum*. Anti-Cancer Agents in Medicinal Chemistry-Anti-Cancer Agents) 2023, 23, 1545–1566.

59. Rizwana, H.; Aljowaie, R.M.; Al Otibi, F.; Alwahibi, M.S.; Alharbi, S.A.; Al Asmari, S.A.; Aldosari, N.S.; Aldehaish, H.A. Antimicrobial and antioxidant potential of the silver nanoparticles synthesized using aqueous extracts of coconut meat (*Cocos nucifera L*). Scientific Reports 2023, 13, 16270.

60. Pasieczna-Patkowska, S.; Cichy, M.; Flieger, J. Application of Fourier transform infrared (FTIR) spectroscopy in characterization of green synthesized nanoparticles. Molecules 2025, 30, 684.

61. Kermen, E.; Kelle, K.; Yilmaz, H.Y.; Küçük, D.; Erden Kopar, E. Biological and Photocatalytic Activities of Green-Synthesized Silver Nanoparticles From *Althaea officinalis* Flowers. Journal of Chemistry 2026, 2026, 5465029.

62. Khan, S.; Zahoor, M.; Khan, R.S.; Ikram, M.; Islam, N.U. The impact of silver nanoparticles on the growth of plants: The agriculture applications. Heliyon 2023, 9.

63. Elsherbiny, A.S.; Galal, A.; Ghoneem, K.M.; Salahuddin, N.A. Graphene oxide-based nanocomposites for outstanding eco-friendly antifungal potential against tomato phytopathogens. Biomaterials Advances 2024, 160, 213863.

64. Ameena, S.; Rajesh, N.; Anjum, S.M.; Khadri, H.; Riazunnisa, K.; Mohammed, A.; Kari, Z.A. Antioxidant, antibacterial, and anti-diabetic activity of green synthesized copper nanoparticles of *Cocculus hirsutus* (Menispermaceae). Applied Biochemistry and Biotechnology 2022, 194, 4424–4438.

65. Maruthai, J.; Muthukumarasamy, A.; Baskaran, B. Fabrication and characterization of silver nanoparticles using bract extract of *Musa paradisiaca* for its synergistic combating effect on phytopathogens, free radical scavenging activity, and catalytic efficiency. IET nanobiotechnology 2019, 13, 134-143.

66. Senevirathna, N.; Hassanpour, M.; O'Hara, I.; Karim, A. Extraction, isolation, identification, and characterization of anthocyanin from banana inflorescence by liquid chromatography-mass spectroscopy and its ph sensitivity. Biomimetics 2024, 9, 702.

67. Górka, K.; Kubiński, K. Antifungal activity against human and plant mycopathogens, and green synthesis of silver nanoparticles exhibiting such activity. Applied Sciences 2023, 14, 115.

68. Wen, H.; Shi, H.; Jiang, N.; Qiu, J.; Lin, F.; Kou, Y. Antifungal mechanisms of silver nanoparticles on mycotoxin producing rice false smut fungus. Iscience 2023, 26.

69. Li, L.; Pan, H.; Deng, L.; Qian, G.; Wang, Z.; Li, W.; Zhong, C. The antifungal activity and mechanism of silver nanoparticles against four pathogens causing kiwifruit post-harvest rot. Frontiers in Microbiology 2022, 13, 988633.

70. Rocha, V.; Carvalho, D.; das Neves, J. Insights on nanomaterials-fungi interactions: probing engineering principles for developing antifungal nanomedicines. International Journal of Pharmaceutics 2025, 125978.

71. Mikhailova, E.O. Silver nanoparticles: mechanism of action and probable bio-application. Journal of functional biomaterials 2020, 11, 84.

72. Roy, A.; Bulut, O.; Some, S.; Mandal, A.K.; Yilmaz, M.D. Green synthesis of silver nanoparticles: biomolecule-nanoparticle organizations targeting antimicrobial activity. RSC advances 2019, 9, 2673–2702.

73. Singh, J.; Kumar, A.; Singh, A.; Nayal, A.S.; Pratap, D. Green synthesized silver and zinc oxide nanoparticles with antifungal, DNA protection, DNA cleavage, and cytotoxic activities. Scientific Reports 2026.

74. Priyadarshini, E.; Priyadarshini, S.S.; Cousins, B.G.; Pradhan, N. Metal-Fungus interaction: Review on cellular processes underlying heavy metal detoxification and synthesis of metal nanoparticles. Chemosphere 2021, 274, 129976.

75. Saad, E.; Salem, S.S.; Fouda, A.; Awad, M.A.; El-Gamal, M.S.; Abdo, A.M. New approach for antimicrobial activity and bio-control of various pathogens by biosynthesized copper nanoparticles using endophytic actinomycetes. Journal of Radiation Research and Applied Sciences 2018, 11, 262–270.

76. Karuppannan, S.K.; Dowlath, M.J.H.; Ramachandran, S.; Rajadesingu, S.; Arunachalam, K.D. Interaction of nanomaterials with microbes. In Nano-Bioremediation: Fundamentals and Applications; Elsevier: 2022; pp. 85–109.

77. Dananjaya, S.; Thao, N.T.; Wijerathna, H.; Lee, J.; Edussuriya, M.; Choi, D.; Kumar, R.S. In vitro and in vivo anticandidal efficacy of green synthesized gold nanoparticles using Spirulina maxima polysaccharide. Process Biochemistry 2020, 92, 138–148.

78. Li, W.; Chen, H.; Cheng, J.; Zhang, M.; Xu, Y.; Wang, L.; Zhao, X.; Zhang, J.; Liu, B.; Sun, J. Improving resistance of mango to Colletotrichum gloeosporioides by activating reactive oxygen species and phenylpropane metabolism of Bacillus amyloliquefaciens GSBa-1. Metabolites 2024, 14, 417.

79. Kumari, M.; Giri, V.P.; Pandey, S.; Kumar, M.; Katiyar, R.; Nautiyal, C.S.; Mishra, A. An insight into the mechanism of antifungal activity of biogenic nanoparticles than their chemical counterparts. Pesticide biochemistry and physiology 2019, 157, 45–52.

80. Nasr Azadani, F.; Madani, M.; Karimi, J.; Sepahvand, S. Green synthesis of silver nanoparticles by Fusarium oxysporum and its function against Aspergillus and Fusarium fungi. Indian Journal of Microbiology 2024, 64, 213–224.

81. Putri, R.H.; Wasita, B.; Priyanto, H.; Pamungkasari, E.P.; Cilmiaty, R. Investigating the Effects of the Ethyl Acetate Fraction of Mas Banana Bracts: Suppressing Cell Growth, Promoting Cell Death, and Targeting Specific Molecules in Hela Cells. Tropical Journal of Natural Product Research 2024, 8, 9035.

82. Das, A.; Bindhu, J.; Deepesh, P.; Priya, G.S.; Soundariya, S. In vitro anticancer study of bioactive compound isolated from Musa extract (Musa acuminata). Indian J Public Health Res Dev 2020, 11, 340–346.

83. Harishini, S.; Thiripurasundari, B. Preliminary Study to Explore the Pharmacotherapeutic Efficacy of Ethanolic Extract of Banana Flower. International Journal Of Innovative Research In Technology 2025, 12, 3494–3505.

84. Abotaleb, M.; Samuel, S.M.; Varghese, E.; Varghese, S.; Kubatka, P.; Liskova, A.; Büsselberg, D. Flavonoids in cancer and apoptosis. Cancers 2018, 11, 28.

85. Singh, H.; Du, J.; Yi, T.-H. Green and rapid synthesis of silver nanoparticles using Borago officinalis leaf extract: anticancer and antibacterial activities. Artificial cells, nanomedicine, and biotechnology 2017, 45, 1310–1316.

86. Al-Sheddi, E.S.; Farshori, N.N.; Al-Oqail, M.M.; Al-Massarani, S.M.; Saquib, Q.; Wahab, R.; Musarrat, J.; Al-Khedhairy, A.A.; Siddiqui, M.A. Anticancer potential of green synthesized silver nanoparticles using extract of Nepeta deflersiana against human cervical cancer cells (HeLA). Bioinorganic Chemistry and Applications 2018, 2018, 9390784.

87. Alharbi, N.S.; Alsubhi, N.S. Green synthesis and anticancer activity of silver nanoparticles prepared using fruit extract of Azadirachta indica. Journal of Radiation Research and Applied Sciences 2022, 15, 335–345.

88. Bin-Jumah, M.; Al-Abdan, M.; Albasher, G.; Alarifi, S. Effects of green silver nanoparticles on apoptosis and oxidative stress in normal and cancerous human hepatic cells in vitro. International journal of nanomedicine 2020, 1537–1548.

89. Ma, W.; He, S.; Ma, H.; Jiang, H.; Yan, N.; Zhu, L.; Bang, J.J.; Li, P.A.; Jia, S. Silver nanoparticle exposure causes pulmonary structural damage and mitochondrial dynamic imbalance in the rat: protective effects of sodium selenite. International Journal of Nanomedicine 2020, 633–645.

90. Lang, Y.; Gao, N.; Zang, Z.; Meng, X.; Lin, Y.; Yang, S.; Yang, Y.; Jin, Z.; Li, B. Classification and antioxidant assays of polyphenols: A review. Journal of Future Foods 2024, 4, 193-204.

91. Alcazar-Fuoli, L.; Mellado, E. Ergosterol biosynthesis in Aspergillus fumigatus: its relevance as an antifungal target and role in antifungal drug resistance. Frontiers in microbiology 2013, 3, 439.

92. Shrivastava, M.; Sharma, P.; Singh, R. Identification of potential CYP51 inhibiting anti-Aspergillus phytochemicals using molecular docking and ADME/T studies. Chemical Biology Letters 2021, 8, 18-21.

Acknowledgements

The authors extend their sincere appreciation and acknowledge the Ongoing Research Funding Program (ORF-2026–1048), King Saud University, Riyadh, Saudi Arabia.

Authors' Contributions: H.R. designed the study, wrote the manuscript, interpreted the results and carried out statistical analysis; A.R. performed nanosynthesis, conducted the antioxidant assay, handled software, and compiled results. R.M.S. provided the methodology, conducted the MTT assay and nanoparticle characterization, helped in writing and assisted in statistical analysis; H.A.D. assisted in nanoparticle characterization, contributed towards the preparation of samples, in vitro studies, preparation for electron microscopy, resources, software, and supervised the work; A.A.T. carried out the antifungal assay, prepared the samples for electron microscopy studies and assisted in statistical analysis; R.B. contributed to conceptualization, carried out molecular docking, and edited the manuscript; All the authors have read the manuscript.

Competing interests: "The authors declare no competing interest."

Funding

The authors extend their sincere appreciation to Ongoing Research Funding Program (ORF-2026–1048), King Saud University, Riyadh, Saudi Arabia

Supplementary Materials: The following supporting information have been uploaded: Figure S1 and Table S1.

Supplementary Files

This is a list of supplementary files associated with this preprint. Click to download.

- SupplementaryfileTableS1andFigureS1.docx